Intelligent real-time multi-functional packaging of rainbow trout fillet containing anthocyanin-rich Althaea Officinalis extract encapsulated with poly (vinyl alcohol) electrospun nanofiber mats

Negar Roshani-Dehlaghi
Islamic Azad University, Tehran
Mohammad Ekrami
University of Tehran
Zahra Emam-Djomeh
emamj@ut.ac.ir

University of Tehran
Shima Yousefi
Islamic Azad University, Tehran

Research Article

Keywords: Althaea Officinalis, Electrospun nanofibers, Freshness monitoring, Multi-functional label, Real-time, Rainbow trout fillet

Posted Date: July 13th, 2024

DOI: https://doi.org/10.21203/rs.3.rs-4577355/v1

Additional Declarations: No competing interests reported.

Abstract

The current study was conducted to fabricate poly(vinyl alcohol) (PVA) electrospun nanofiber mats containing anthocyanin-rich *Althaea Officinalis* extract (AO_{EX}; 5, 10, 15 and 20%v/v) to monitor the spoilage and enhance the shelf-life quality of rainbow trout fillet. The AO_{EX} displayed colour change when subjected to the different pH buffer solutions. The optimum conditions for fabricating PVA nanofibers with a minimum diameter (204.9 nm) were found using response surface methodology (RSM). The viscosity, electrical conductivity and surface tension of PVA-AO_{EX} solutions were significantly changed up to 993.2 cp, 1275.65 μS/cm and 54.16 mN/m, respectively, by increasing AO_{EX} content. The IC_{50} values for DPPH and ABTS radical scavenging by AO_{EX} were 375 and 800 ppm, respectively. The phytochemical and antibacterial properties of PVA-AO_{EX} were improved by adding AO_{EX} content. Microscopic images confirmed the increase in the diameter and roughness of PVA-AO_{EX} nanofibers by adding the AO_{EX} up to 480.9 nm. After the addition of AO_{EX}, the PVA-AO_{EX} nanofibers become more hydrophilic (θ = 47.6–73.1°), but the melting temperature (T_m) values of the PVA-AO_{EX} nanofiber mats have decreased (217.6°C). Fourier-transform infrared spectroscopy (FTIR) showed that adding AO_{EX} and electrospinning process does not have a negative effect on the structure of the PVA. The PVA-AO_{EX} nanofibers mats, revealing that the real-time multi-functional innovative packaging changed colour from white to brown and, at the same time, exceeded the total viable count (TVC) and total volatile basic nitrogen (TVB-N) acceptance limit of rainbow trout fillet.

1. Introduction

Innovative packaging enables real-time data on the quality and freshness of packaged food items, safeguarding customers from foodborne illnesses. Colourimetric pH-responsive indicators have been widely used in intelligent food packaging due to their ability to quickly monitor the microbiological decomposition of high-protein and high-fat food (Shakouri et al. 2023). These indicators are generally affordable and non-destructive. Extensive research has been conducted on producing and analysing colour indicators, often using a pH-sensitive chemical dye or natural colourant combined with a polymer matrix. Anthocyanins have been chosen over synthetic dyes to create intelligent packaging in this situation because of their advantages in terms of human health and environmental sustainability (Alizadeh-Sani et al. 2020). Prior research has concentrated chiefly on using natural colours derived from red cabbage (Abedi-Firoozjah et al. 2022), purple cabbage (He et al. 2022), carrot (Goodarzi et al. 2020), jaboticaba (Hoffmann et al. 2022), barberry (Alizadeh-Sani et al. 2021b) and saffron (Ekrami et al. 2022e) for the production of intelligent pH-sensitive indicators.

Althaea officinalis is a medicinal plant used to treat conditions such as lipemia, inflammation of the nasal and oral canals, stomach ulcers, platelet aggregation, cystitis, and irritating coughs. This plant is a member of the *Malvaceae* family and is primarily found in moist regions, particularly in southern Europe, Iran, Iraq, and Turkey (Mahboubi 2020). The petals exhibit a colour palette ranging from light pink to reddish pink, with occasional instances of white. *Althaea officinalis* is a plant that contains anthocyanins

and hydrocolloids (Karimi et al. 2021). Recent studies have discovered Quercetin, flavonol glycosides, and phenolic acids as the main constituents of Althaea officinalis. These components are well-known for their antibacterial and antioxidant effects (Xue et al. 2023).

There is a link between antioxidant activity and the intensity of the plant's colour. The researcher has reported a potential correlation between the antioxidant activity and the hue. Pigmented plants are excellent reservoirs of antioxidant chemicals (Bonaterra et al. 2020). Hence, plants exhibiting vibrant hues are ideal options for enhancing antioxidant activity. Anthocyanins are potent antioxidants that provide colour to most flowers, fruits, and vegetables (Tena et al. 2020). Anthocyanins are responsible for the pigmentation in plants, giving rise to red, purple, and blue hues. Hence, a potential correlation exists between the anthocyanin concentration in the intense pigmentation of plants and their ability to neutralise oxidising agents. The *Althaea officinalis* extract demonstrated potent antioxidant activity in many antioxidant assays, attributed to the presence of bioactive components such as flavonols, flavones, flavanone, anthocyanins, and catechins (Bohdanovych et al. 2023).

Various biodegradable polymers derived from proteins, polysaccharides, and gums have been used as a matrix to immobilise the anthocyanins. The selection of the matrix is crucial for the development of intelligent pH-sensitive indicators. The functional packaging nanofiber mats must possess sensitivity to a broad spectrum of pH values and exhibit quick reactivity towards gaseous amines emitted by contaminated food (Ekrami et al. 2022d). Electrospinning is an innovative nanotechnology method used to encapsulate natural colours. It includes using high voltage to stimulate charged polymer chains in a solution that is flowing consistently. The solvent is then evaporated to produce electrospun nanofibers, which are collected (Emam-Djomeh et al. 2023). The generated electrospun nanofibers possess a significant ratio of surface area to mass, low density, a highly porous structure, and long-lasting effectiveness against harmful/bacterial decay (Ekrami et al. 2022b).

Poly(vinyl alcohol) (PVA) is considered an essential and cost-effective natural resource due to its favourable material characteristics, such as being non-toxic, biocompatible, biodegradable, and possessing high tensile strength and flexibility (Emam-Djomeh et al. 2023).

As far as we know, no research has been conducted on using anthocyanin-rich *Althaea Officinalis* extract (AO_{EX}) to create pH-sensing intelligent packaging electrospun nanofibers to monitor and slow down food spoiling. Hence, this research aimed to encapsulate AO_{EX} into PVA nanofiber mats using the electrospinning technique. Additionally, it aimed to monitor the freshness and improve the quality of rainbow trout fillets throughout 14 days of refrigerated storage (Fig. 1).

2. Materials and Methods

2.1. Materials

Althaea Officinalis flowers and fresh rainbow trout (*Oncorhynchus mykiss*) fillets were provided from Karaj, Iran. The commercial PVA (medium molecular weight = 72000 Da) was purchased from Merck, Germany. 2, 2-diphenyl-1-picrylhydrazyl (DPPH), 2, 20 –azinobis (3-ethylbenzothiazoline- 6- sulfonic acid) (ABTS), and Folin-Ciocalteu were purchased from Sigma-Aldrich, USA. The microbiological growth medium (brain heart infusion (BHI) broth, trypton soy agar (TSA), mueller-hinton agar (MHA) and plate count agar (PCA)) purchased from QUELAB, Canada. All the other solvents and chemicals used in this research were of analytical grade.

2.2. Extraction of Anthocyanin-Rich Extract

After separating the stem from the *Althaea Officinalis* flowers, the petals were covered, placed away from sunlight, and dried at room temperature. Crushed dried petals were sieved (40 meshes) and stored in dark vials at 4°C. The anthocyanin-rich extract extraction was performed using the procedure described by Ekrami et al. (2022) with slight modifications. Powdered flower petals were combined with distilled water: ethanol (75:25 v/v), at a ratio of 1:20 (w/v), for 24 h before being centrifuged for 10 min at 5000 g to remove any remaining solids. After the solvent was evaporated from the extract using a rotary evaporator (IKA, Germany) set at 37°C, the resulting filtrate was kept in a dark container in the refrigerator.

Preparation and Characterisation of Electrospinning Solutions

PVA (10%w/v) was dissolved in distilled water at 80°C for 1 h and kept for 24 h at 4°C (Ebadi Ghareh Koureh et al. 2023). To prepare PVA-AO_{EX} solutions, AO_{EX} (5, 10, 15 and 20%v/v based on solution volume) was added to the PVA solution, stirred for 10 min at 300 rpm and then sonicated using a probe ultrasound (Hielscher, Germany) at 24 kHz, amplitude 50%, duty cycle 0.5 for 5 min) on ice followed by 30 min rest to remove air bubbles.

The surface tension of each electrospinning solution was determined using a digital tensiometer (Kruss, Germany) based on the Wilhelmy plate method [34]. 40 g of the solutions were poured into a 70 mm diameter glass beaker, previously rinsed with absolute ethanol, deionised, and double distilled water and dried at 70°C overnight to remove any surface-active material. Solutions were then equilibrated to 25°C, and the platinum plate was lowered into the dispersion to form a meniscus. The surface tension was calculated in mN/m using Eq. (1):

$$\sigma = \mathbf{F}/\mathbf{L} \times \mathbf{cos}\backslash\mathrm{varvec}\theta \quad \textbf{(1)}$$

Where σ is surface tension, F is the force acting on the platinum plate, L is the length of the total meniscus (2 × the length + thickness), and θ is the contact angle.

The dynamic viscosities of the electrospinning solutions were analysed using a shear capillary rheometer (Brookfield, USA) at 25°C. Shear viscosity was determined as a function of shear rate ranging from 1 to 1000 s^{-1} with ten measurements per decade. Electrical conductivity was determined at 25°C using a portable conductivity meter (WTW, Germany).

2.3. Electrospinning process

A horizontal electrospinning apparatus was employed at 25 ± 1°C and a 30–35% relative humidity. This system consisted of a dosing pump (Terumo, Tokyo, Japan) with a feeding rate of 0.01-10 mL/h equipped with a 1 mL syringe with a 21 G needle head and high voltage supply (input 220 V AC up to 30 kV DC output). The positive electrodes were connected to the needle's tip, and an aluminium foil attached to the cylindrical rotating collector was connected as a negative electrode.

The three independent variables (pump rate, distance between tip and collector, and high voltage) were used to determine the finest PVA nanofiber diameter using a five-level central composite design (CCD) approach-based response surface methodology (RSM) analysis (data not shown). The effect of input factors (independent variables) on the diameter and desirability of the optimum conditions for fabricating PVA nanofibers is presented in Fig. 2.

The optimum conditions for fabricating PVA nanofibers with a minimum diameter (204.9 nm) were the distance between tip to collector 17.5 cm, an applied voltage of 20 kV, and a pump rate of 1 mL/h. PVA-AO_{EX} nanofiber mats electrospuned under optimum conditions of fabricating PVA nanofibers.

Phytochemical Properties

Antioxidant Activity

To test the antioxidant activity of AO_{EX}, two protocols were considered: (a) reduction in the radical DPPH and reduction in the radical ABTS according to Abd-ElGawad et al. (2022) (Abd-ElGawad et al. 2022) with some modifications. In the DPPH and ABTS assay, the AO_{EX} and standard antioxidant (ascorbic acid) were prepared in a 5–5000 ppm concentration range, using methanol as a solvent. This range was selected based on the scavenging activity that enabled us to determine the IC_{50} (AO_{EX} amount necessary to reduce the radical by 50%). To perform the DPPH assay, equal volumes of each concentration and DPPH (0.3 mM) were shaken vigorously and kept in dark conditions for 30 min. The absorbance was assessed at 517 nm via UV-VIS spectrophotometer (CECIL, England).

To conduct the ABTS assay, about 0.2 mL of each concentration was mixed with 2 mL of freshly prepared ABTS and incubated in a dark condition for 6 min. The colour absorbance was measured at 734 nm by UV-VIS spectrophotometer.

The DPPH and ABTS radical scavenging activity (RSA) was then calculated according to the following Eq. (2):

$$\mathbf{RSA}\,(\%) = (1 - (\mathbf{A_s}/\mathbf{A_C})) \times 100$$

2

Here, A_C is the absorbance of the control, and A_S is the absorbance of the sample.

Total Phenolic Content (TPC)

The TPC of AO_{EX} and PVA-AO_{EX} nanofiber mats were measured using the Folin-Ciocalteu method, as reported by Mirzakhani et al. (2018), with minor changes (Mirzakhani et al. 2018). An aliquot of 2 mL of 10%v/v Folin-Ciocalteu reagent was added to 0.5 mL of extract and stored in the dark for 3 min. Then, 2.5 mL of sodium carbonate solution (7.5%w/v) was added to the mixture and kept in the dark at 25°C. Finally, the absorbance of the sample was measured by UV-VIS spectrophotometer at 765 nm. A standard curve (0-100 µg/mL) was plotted using gallic acid as a standard. The TPC was then reported as mg of gallic acid (GAE), equivalent to 100 g of sample.

Total Anthocyanin Content (TAC)

The pH-differential method measured the TAC of AO_{EX} and PVA-AO_{EX} nanofiber mats, as reported by Sutharut et al. (2012), with minor changes (Sutharut and Sudarat 2012). Measure the absorbance of each dilution at 510 and 700 nm against a blank cell filled with distilled water. Absorbance readings are done against water blanks. The absorbance of the diluted sample (A) was calculated in Eq. (3):

$$\mathbf{A} = (\mathbf{A}_{510} - \mathbf{A}_{700})_{\mathbf{pH1}} - (\mathbf{A}_{510} - \mathbf{A}_{700})_{\mathbf{pH4.5}}$$

3

The monomeric anthocyanin pigment concentration in the original sample was calculated in Eq. (4):

$$\mathbf{TAC} = (\mathbf{A} \times \mathbf{MW} \times \mathbf{DF} \times \mathbf{V} \times 1000)/(\varepsilon \times \mathbf{W} \times \mathbf{L})$$

4

Where TAC is total anthocyanin content, A is the absorbance, MW is the molecular weight of cyanidin-3-glucoside (449.2 g/mol), DF is the dilution factor, V is the solvent volume (mL), ε is the molar absorptivity (26,900 L/mol cm), W is sample weight (mg), and L is the cell path length (1 cm). The TAC was expressed as mg cyanidin-3-glucoside equivalents (CGE) per 100 g sample.

Total Flavonoid Content (TFC)

The procedure described by Habibi et al. (2015) was pursued to determine the TFC of AO_{EX} and PVA-AO_{EX} nanofiber mats (Habibi et al. 2015). In brief, the sample was diluted with methanol until 100 µg/mL. The calibration curve was prepared by diluting Quercetin (QUE) in methanol (0–100 µg/mL). The diluted extract or QUE (2.0 mL) was mixed with 0.1 mL of 10%w/v aluminium chloride solution and 0.1 mL of 0.1 mM potassium acetate solution. The mixture was kept at room temperature for 30 min. Then, the maximum absorbance of the mixture was measured at 415 nm using a UV–VIS spectrophotometer. The TFC was expressed as mg QUE/100 g.

Ferric Reducing Antioxidant Power (FRAP)

With due attention to the TPTZ method described by Zhang et al. (2023), using Trolox as a standard of the calibration curve, FRAP of AO_{EX} and PVA-AO_{EX} nanofiber mats was performed. The FRAP stock solution was made by mixing sodium acetate buffer (0.3 M, pH 3.6), $FeCl_3$ solution (0.02 M), and TPTZ solution (0.01 M, in 0.04 M HCl) in a 10:1:1 vol ratio, respectively. The FRAP stock solution was freshly prepared and stored at 37°C for 1 h before use. The sample (10 µL) was added to the FRAP solution (190 µL) in a 96-well microplate, and the mixture was incubated at room temperature for 30 min. The absorbance of the samples was measured at 593 nm using a UV–VIS spectrophotometer (Zhang et al. 2023). The results were expressed as µmol Trolox equivalent (TRE)/100 g.

Antibacterial Properties

Escherichia coli O157:H7 (PTCC No. 1535), *Staphylococcus aureus* (PTCC No. 1112), *Pseudomonas aeruginosa* (PTCC No. 1310) and *Bacillus cereus* (PTCC No. 1015) were used as model food spoilage or pathogenic microorganisms. The bacteria were incubated overnight at 37°C on a BHI medium. The antibacterial activity of the PVA-AO_{EX} nanofiber mats was then determined using the agar disc diffusion assay, according to the method described by Ekrami et al. (2022), with some modifications. Suspensions of the microorganisms (1–5 10^8 CFU/mL) were placed on the surfaces of the TSA medium. Measurements of the dimensions of the inhibition zones were used to establish the antibacterial efficacy of the different microbial strains. For this experiment, 6 mm diameter disks of nanofiber mats were cut and sterilised by UV irradiation for 30 s, placed on MHA medium, and then incubated at 37°C for 18 h (Ekrami et al. 2022a).

pH Sensitivity and Color Parameters

The pH of AO_{EX} solutions was controlled by different buffers (2.5, 7 and 13.5), and sensitivity was determined via the UV-VIS spectrophotometer at 400–800 nm wavelengths. The colour parameters were taken digitally, and their colours were evaluated using an instrumental colourimeter (Minolta, Japan) after being calibrated against a white plate. Using the colour coordinates L or lightness (black = 0 to white = 100), a (greenness = -60 to redness = + 60) and b (blueness = -60 to yellowness = + 60), the following Eq. (5–7) are used to calculate the total colour difference (ΔE), whitish (WI), and yellowness (YI) indices of samples, respectively (Ekrami et al. 2022c):

$$\Delta E = \sqrt{(\mathbf{L}-\mathbf{L}')^2+(\mathbf{a}-\mathbf{a}')^2+(\mathbf{b}-\mathbf{b}')^2} \quad (5)$$

$$WI = 100 - \sqrt{(100-\mathbf{L})^2+\mathbf{a}^2+\mathbf{b}^2} \quad (6)$$

$$YI = 142.86 \times \mathbf{b}/\mathbf{L} \quad (7)$$

Morphology

Scanning Electron Microscopy (SEM)

A scanning electron microscope (TESCAN, Czech Republic) was used to assess the effects of AO_{EX} on the microstructure of PVA nanofiber mats. The PVA-AO_{EX} nanofiber mats were broken in liquid nitrogen, then fixed on an aluminium stub using adhesive tape and spluttered with gold using a sputter coater (Balzers, Liechtenstein) before visualisation. The observation was conducted at 20 kV acceleration potential.

Atomic Force Microscopy (AFM)

The morphological properties of PVA-AO_{EX} nanofiber mats were examined by tapping mode atomic force microscope (DME, Denmark) with an E-type scanner. The rectangular silicon cantilever was employed with a nominal spring constant of 5–100 N/m and nominal resonance frequencies of 10–320 kHz. The NanoScope software is employed for all AFM image processing.

Wettability

The contact angle was measured using the sessile drop technique to establish the wettability of PVA-AO_{EX} nanofiber mats. An optical goniometer (PG-X, Switzerland) was used to determine the contact angle between the surfaces of the produced films and water. In brief, placed a droplet of distilled water (4 µL) on the indicator films and measured the droplet's angle.

Differential Scanning Calorimetry (DSC)

Thermal analysis was conducted on a differential scanning calorimeter (Rigaku, Japan) under a nitrogen atmosphere. Each nanofiber mat was accurately weighed (3 mg) and sealed in an aluminium crucible. Afterwards, the sample was heated from 25°C to 325°C at a heating rate of 10°C/min. The melting temperature (T_m) was determined from the resulting thermogram. This temperature was considered the middle point of the beginning and end of the curve changes in heat flow.

FTIR

The Nicolet spectrometer (Perkin Elmer, USA) was utilized to acquire the FTIR spectra of PVA, AO_{EX} and PVA-AO_{EX} nanofiber mats. The scanning process was conducted multiple times within the range of 4000–400 cm^{-1}.

Evaluation of Fish Freshness

Preparation of Samples

Fresh rainbow trout was chopped as fillets into strips after removing the intestines, head, skin, tail, and scale, and 15 g were immediately put in Petri dishes. The Petri dishes were kept in a refrigerator at 4°C after the PVA-AO_{EX} nanofiber mats (10%v/v) as real-time multi-functional innovative packaging were coated on the fish fillet samples. A digital camera was used to record the colour shift of the intelligent packaging.

pH Measurement

The pH values were determined according to Li et al. (2013). During the time intervals, pH values of fish samples were checked after vigorous homogenisation (IKA, Germany) at 12000 rpm of 10 g of sample in 90 mL distilled water by a digital pH meter (IKA, Germany) (Li et al. 2013).

Total Volatile Basic Nitrogen (TVB-N)

The TVB-N level in the fish sample was determined using the technique developed by Zhai et al. (2017) with some modifications (Zhai et al. 2017)—a homogeniser ground 10 g of the fish sample with 100 mL of distilled water. The homogenate was then filtered using filter paper. The filtrate was mixed with 5 mL of 1% magnesium oxide solution (1 g/L) in the reaction chamber. Distilled water was utilised as a blank control to replace the fish filtrate. Following the completion of the reaction, the boric acid solution was titrated with 0.01 M hydrochloric acid solution until the colour changed to blue-violet. The TVB-N (mg/100 g) level was determined using the following Eq. (8):

$$\mathrm{TVB-N} = ((\mathrm{V_1} - \mathrm{V_2}) \times \mathrm{C} \times 14/\mathrm{m} \times 0.05) \times 100$$

8

Where V_1 is the volume of hydrochloric acid consumed by the sample (mL); V_2 is the volume of hydrochloric acid consumed in the blank (mL); C is the concentration of hydrochloric acid (M); m is the sample quality (g).

Microbial Analysis

The fish sample's total viable count (TVC) was determined using a modified Jiang et al. (2020) technique. In summary, 10 g of each fish sample was first finely chopped and grounded. Subsequently, it was transferred into 90 mL sterilised 0.90% saline solution and homogenised at 12000 rpm for 2 min. Then, for microbial counting, 1 mL of each dilution was mixed with PCA medium in Petri dishes and incubated at 37°C for 48 h. The TVC was calculated by counting the number of colony-forming units (Jiang et al. 2020).

Statistical Analysis

Design Expert software v12 was used to design the central combination experiment following the acquired experimental variables. Data was analysed using SPSS v18 (SPSS Inc., Chicago, Ill., USA). One-way analysis of variance (ANOVA) and Duncan's test at a 95% confidence level ($p < 0.05$) were used to determine the significant difference between the averages of treatments. Three replications were used in the experiments.

Result and Discussion

Electrospinning Solution Characterization

Solution properties like viscosity, surface tension and electrical conductivity of electrospinning solution, process parameters such as applied voltage, volume feed rate, needle diameter and distance between needle and collector, as well as environmental conditions, mainly temperature and humidity are influential factors on the success of electrospinning process and morphological characteristics of fabricated fibrous mats. Furthermore, those solution properties depend on the type of solvent and polymer as well as the concentration of polymer; therefore, it is crucial to determine the optimum properties of the electrospinning solution. In this regard, the properties of PVA and PVA-AO_{EX} solutions are presented in Table 1. Viscosity could determine the degree of polymer chain entanglements in the solution. Very low viscosity nor very high viscosity solutions will allow continuous fibre formation due to the difficulty of ejecting jets from polymer solutions. The dominant morphologies for polymeric solutions with low viscosity are those with beads. Increasing the viscosity of polymer solutions significantly reduces bead formation, and fibres become relatively fine and smooth. Spindle-shaped beads formation above the critical viscosity point may be attributed to the disconnection of the current flow between the needle and collector or less stretching of the stream. Consequently, it is important to use a polymer solution with optimum viscosity to fabricate bead-free fibers.

For all solutions, a rise in shear rate caused a decrease in apparent viscosity (Fig. 3). The decline rate of the apparent viscosity was lower with increasing AO_{EX} content. All samples were pseudoplastic or could be diluted by shear (n 1). Fitting different rheological models to the shear stress–shear rate data showed that the power-law model best fitted to the rheological data of PVA-AO_{EX} solutions.

According to Table 1, the viscosity of pure PVA solution was 702.6 ± 12.8 cp. The viscosity of PVA-AO_{EX} solutions was significantly increased up to 993.2 ± 17.5 cp. by increasing AO_{EX} content. The increase might be attributed to AO_{EX} viscosity, which was higher than the viscosity of PVA solution.

The anthocyanin appeared to reduce the tendency for the network to form, thereby significantly reducing the viscosity of the emulsions so that it was closer to that of the oil phase (Liu et al. 2019). However, in our research, the viscosity increased by adding the AO_{EX}. As expected, the hydrocolloids present in the AO_{EX} have a positive effect in increasing the viscosity of the solution.

Tabarsa et al. (2017) reported the polysaccharide from the *Althaea Officinalis* flower was determined to be an acidic, rhamnose-rich polymer. Glucose, galactose, and arabinose residues randomly occurred in the hydrocolloid chain. Aqueous dispersions of AO_{EX} hydrocolloids showed a low-shear Newtonian plateau and pseudoplastic flow behaviour at higher shear. hydrocolloids flow and viscoselastic behaviors were dependent on solution concentration (Tabarsa et al. 2017). Also, Mousavi et al. (2019) introduced *Althaea Officinalis* flower mucilage as hydrocolloid with a complex polymer with the nature of a carbohydrate having branched structures and soluble hydrophilic polysaccharides, which act as thick and sticky substances in solutions (Mousavi et al. 2019).

Table 1
Characterisation of PVA and PVA-AO_{EX} electrospinning solutions

AO_{EX} (%v/v)	Viscosity (cp)	Electrical conductivity (µS/cm)	Surface tension (mN/m)
0 (PVA)	702.6 ± 12.8^{d}	3443.68 ± 35.72^{a}	62.67 ± 0.32^{a}
5	711.4 ± 10.6^{d}	3160.74 ± 23.43^{b}	61.33 ± 0.20^{b}
10	758.1 ± 8.3^{c}	2540.18 ± 32.60^{c}	58.63 ± 0.25^{c}
15	957.7 ± 13.4^{b}	1937.62 ± 25.84^{d}	56.40 ± 0.26^{d}
20	993.2 ± 17.5^{a}	1275.65 ± 52.04^{e}	54.16 ± 0.20^{e}

*Means with different letters within a raw are significantly different ($p < 0.05$).

pH Dependence of AO_{EX}

The colour variation of AO_{EX} buffer solutions with pH 2.5, 7 and 13.5 was measured with UV–VIS spectra to verify the usefulness of the AO_{EX} as a sensitive indicator dye. As shown in Fig. 4A, the colour of AO_{EX} solution changed from bright red to yellow with increasing pH. The AO_{EX} solution appears red at pH 2.5, gradually changing from red to light pink at pH 7, and the yellow colour gradually changes to brown at pH 13.5.

As the pH was adjusted from acidic to alkaline, the solutions went from red to yellow, and many other hues appeared at intermediate pH levels. Different anthocyanin molecules undergo structural alterations at different pH levels, resulting in different colours: flavylium cation (pH 3), carbinol pseudo-base (pH 4–5), quinonoidal anhydrous-base (pH 6–8), and chalcone (pH > 10) (Zhang et al. 2019). The anthocyanin solutions' maximum absorption peak strength and wavelength were pH-dependent (Fig. 4B). At a pH of 2.5, the absorbance peaked at 520 nm, but the peak weakened when the pH was raised. When the pH was adjusted to pH = 7, a new peak appeared at 540 nm, and the intensity and location of this peak grew when the pH was increased. This is a hallmark property of anthocyanins. When the pH was increased to pH = 13.5, the strength of this peak decreased, and a new, faint peak emerged at 410 nm. It has already been shown that variations in the molecular species present account for the shifts in absorbance spectra and colour in saffron anthocyanin solutions. As mentioned earlier, the change in absorbance spectra and colour of the anthocyanin solutions can be attributed to changes in the molecular species present. Similar findings have been reported for anthocyanins isolated from the roselle (Lv et al. 2024) and saffron (Ekrami et al. 2022e). The above results prove that AO_{EX} can be used as a natural pH indicator in innovative packaging by continuously transforming their structures under different pH environmental conditions.

3.5. Phytochemical and Antibacterial Properties

In previous studies, it was reported that the levels of antioxidant activity and content of total phenolics, total anthocyanins, total soluble solids, glucose, fructose, and acidity were higher in plants in the Mediterranean climate compared with those grown in the desert climate (Krüger et al. 2021).

The DPPH and ABTS methods are appropriate and approved ways to measure the antioxidant activity of essential oils and extracts. This method is based on trapping the amount of free radicals DPPH and ABTS using antioxidant agents. The present results in Fig. 5 show that the AO_{EX} has an extraordinary activity in trapping free radicals. The AO_{EX} at a concentration of 50 ppm trapped 19.33% and 10.50% of the available DDPPH and ABTS free radicals, respectively. At the concentration of 500 ppm, the activity of the AO_{EX} increased and showed an increase of 55.47% and 41.88% in the DPPH and ABTS free radical scavenging rate, respectively. At a concentration of 5000 ppm, the AO_{EX} inhibits 75.87% and 60.61% of DPPH and ABTS free radicals, respectively. This shows that the antioxidant activity of AO_{EX} increases in a dose-dependent manner. Figure 5 also shows the result of calculating the IC_{50} of AO_{EX} compared to ascorbic acid as a positive control and the standard index for measuring the amount of IC_{50}. The IC_{50} values of DPPH and ABTS provided for ascorbic acid were 20 and 37.5 ppm, respectively, while these values were 375 and 800 ppm for AO_{EX}. This shows that compared to ascorbic acid, AO_{EX} shows less antioxidant activity, which is expected. Tabarsaa et al. (2017) reported that the IC50 of the polysaccharide fraction of Althaea Officinalis was 4770 ppm (Tabarsa et al. 2017). Polyphenols, especially anthocyanins, are known as powerful antioxidants. The mechanism of action of these compounds is multidirectional: free radical scavenging, chelation of transition metal ions (copper, iron), inhibition of enzymes involved in forming reactive oxygen species (ROS), induction of endogenous antioxidant enzymes, and prevention of lipid peroxidation. Generally, the antioxidant activity of anthocyanins is associated with the number of free hydroxyls around the pyrone ring. A more significant number of hydroxyls has more excellent antioxidant activity. Anthocyanins with their 3',4'-dihydroxy groups can quickly chelate metal ions to form stable anthocyanin-metal complexes; for instance, delphinidin is the most active against the superoxide anion (being followed by cyanidin and pelargonidin), and pelargonidin is the most efficient against the hydroxyl radical (Miguel 2011).

The results of the phytochemical analysis of AO_{EX} and PVA-AO_{EX} nanofiber mats are described in Table 2. The TAC, TPC, TFC and FRAP of AO_{EX} were found to be 419.2 mg CGE/100 g, 29.9 mg GAE/100 g, 52.52 mg QUE/100 g and 15.70 µmol TRE/100 g, respectively. Sadighara et al. (2012) reported the reddish pink flowers of *Althaea Officinalis* **to** have more antioxidant activity (CUPric reducing antioxidant capacity and ferric iron-reducing assay) and flavonoid content (Sadighara et al. 2012). Elmastas et al. (2004) results indicate that the ethanol extract of marshmallows has significant antioxidant activity against various antioxidant systems in vitro. Moreover, marshmallow can be an easily accessible source of natural antioxidants in food and pharmaceutical industries. The various antioxidant mechanisms of ethanol extract from marshmallow may be attributed to strong hydrogen donating ability, metal chelating ability, and their effectiveness as good scavengers of superoxide and free radicals (Elmastas et al.

2004). PAŞCA et al. (2016) results show small marshmallow (*Althaea officinalis*) can be considered melliferous plants for their high biologically active compounds potential, and bee products (honey and pollen) having the composition of these plants could have high antioxidant and antibacterial properties (PAŞCA et al. 2016) The beneficial effects of phenolic compounds have been attributed to their antioxidant activity (Omidi et al. 2014). This effect can be attributed to the presence of a high level of phenolic groups in the structure of the anthocyanin molecules (Alizadeh-Sani et al. 2021a).

The antioxidant activity of PVA-AO_{EX} nanofiber mats was dose-dependently linked to the increase in all three oxidation markers when the AO_{EX} content was increased ($p < 0.05$). Similar studies have shown that adding anthocyanin extract effectively improved the antioxidant ability of the nanofibers (Duan et al. 2021; Ahmed et al. 2023; Alizadeh-Sani et al. 2021a).

Testing the efficacy of the PVA-AO_{EX} nanofiber mats against both Gram-positive and Gram-negative bacterial strains helped investigate the antibacterial activity (Table 2). Because the control film could not inhibit the growth of either strain of bacteria, it became clear that PVA nanofibers lacked antibacterial qualities. PVA-AO_{EX} nanofiber mats inhibited the growth of both bacteria in a dose-dependent manner, with greater efficacy against *Staphylococcus aureus*. AO_{EX} seem to have bactericidal effects due to highly antimicrobial chemicals such as anthocyanins. Similar studies have shown that many plant anthocyanins have specific bacteriostatic effects in addition to their effects on virulence genes and antibiotic resistance, such as red rose (Saati et al. 2018), *Thymus kotschyanus* boiss & hohen (Baharfar et al. 2015), *Aronia melanocarpa* (Deng et al. 2021), black and non-black mulberries (Chen et al. 2017) and *Clitoria ternatea* (Jeyaraj et al. 2022). Anthocyanins have significant antibacterial activity, which damages the cell membrane and affects AKP, ATPase and SOD. Anthocyanins also may decrease the TCA cycle and the biosynthesis of pathogens, leading to bacterial decomposition and eventual death (Sun et al. 2018). As a result, the ability of bioactive components in the AO_{EX} to penetrate the cells and interact with their key constituents differs for the two kinds of bacteria. As a result of variations in their cell wall composition and architecture, PVA-AO_{EX} nanofiber mats were more efficient against Gram-positive than Gram-negative bacteria. Unlike Gram-negative bacteria, which have a phospholipid bilayer with connected lipopolysaccharides, Gram-positive bacteria have a thick outer coating of peptidoglycan (Ekrami et al. 2019).

Table 2
Phytochemical and antibacterial properties of AO_{EX} and PVA-AO_{EX} nanofiber mats

Phytochemical properties	**PVA-AO_{EX} nanofiber mats (%v/v)**				
	0 (Control)	**5**	**10**	**15**	**20**
TPC (mg GAE/100 g)	0.00 ± 0.00^{e}	2.09 ± 0.37^{d}	3.95 ± 0.46^{c}	6.80 ± 0.24^{b}	9.12 ± 0.40^{a}
TAC (mg CGE/100 g)	0.00 ± 0.00^{e}	28.29 ± 1.64^{d}	61.85 ± 3.38^{c}	101.60 ± 3.31^{b}	144.94 ± 6.16^{a}
TFC (mg QUE/100 g)	0.00 ± 0.00^{e}	3.24 ± 1.21^{d}	7.62 ± 1.12^{c}	10.94 ± 1.40^{b}	15.75 ± 1.36^{a}
FRAP (µmol TRE/100 g)	0.00 ± 0.00^{d}	7.19 ± 0.99^{c}	11.33 ± 1.20^{b}	15.70 ± 1.25^{a}	17.21 ± 1.10^{a}
Inhibition zone diameters (mm)					
Staphylococcus aureus	0.00 ± 0.00^{e}	6.71 ± 0.13^{d}	7.81 ± 0.29^{c}	10.46 ± 0.28^{b}	13.32 ± 0.216^{a}
Escherichia coli O157:H7	0.00 ± 0.00^{d}	5.76 ± 0.33^{c}	6.19 ± 0.37^{c}	7.85 ± 0.17^{b}	8.94 ± 0.34^{a}
Pseudomonas aeruginosa	0.00 ± 0.00^{c}	5.51 ± 0.36^{b}	5.74 ± 0.30^{b}	5.98 ± 0.29^{b}	7.72 ± 0.40^{a}
Bacillus cereus	0.00 ± 0.00^{e}	6.24 ± 0.32^{d}	7.37 ± 0.22^{c}	8.66 ± 0.34^{b}	11.52 ± 0.41^{a}

*Means with different letters within a raw are significantly different ($p < 0.05$).

Colour parameters and pH sensitivity

As mentioned, the colour change of AO_{EX} buffer solutions in response to different pH levels demonstrates their sensitivity to pH (Fig. 4). As the pH was raised from 2.5 to 13.5, the AO_{EX} buffer solutions went from red to yellow. These colour changes are brought on by alterations in the molecular structure and absorption characteristics of anthocyanin molecules, which are triggered by variations in pH (Alizadeh-Sani et al. 2021a).

The colour parameters of PVA-AO_{EX} nanofiber mats with different pH are shown in Fig. 6. When the pH was adjusted to levels below or above 7, their lightness (L*) and WI decreased drastically as the PVA-AO_{EX} nanofiber mats tended to become coloured (increase in ΔE). In fact, with the increase in pH, the colour of the PVA-AO_{EX} nanofiber mats becomes more yellow (increase in b* index) and with the decrease in pH, the colour of the PVA-AO_{EX} nanofiber mats becomes redder (increase in a* index).

According to Tassanawat et al. (2007), a ΔE greater than 5 implies a colour change perceptible by the human eye, essential for developing colourimetric sensors for packaging materials (Tassanawat et al. 2007). As shown in Fig. 6, the ΔE values in the current investigation were more than 5, indicating that the PVA-AO_{EX} nanofiber mats may be employed as pH-sensitive indicators in novel packaging materials.

Microstructure

To investigate the PVA-AO_{EX} nanofiber mats microstructure, SEM (Fig. 7) and AFM (Fig. 8) were used to observe their surfaces. In the electrospinning solution characterisation section, it is mentioned that AO_{EX} contains mucilage as a hydrocolloid structure. Since the primary goal of the current research is to prepare the anthocyanin-rich *Althaea Officinalis* extract, the total amount of mucilage in the AO_{EX} is low; for this reason, the AO_{EX} is not capable of electrospinning and producing nanofibers, and the result was bulky fibres with large beads (Fig. 7A). The morphology of the control (PVA) nanofibers was uniform and smooth, with an average diameter of 204.9 nm (Fig. 7B). The intermolecular forces, including van der Waals, hydrogen bonds, hydrophilic attraction, and electrostatic interactions, bound PVA as biopolymer and AO_{EX} as additive together to form a network (Emam-Djomeh et al. 2015). However, insoluble particulate matter in the AO_{EX}, such as hydrophilic compounds or fibrous plant tissue fragments, was responsible for the minor heterogeneities seen on the PVA-AO_{EX} nanofiber mats surfaces (Fig. 7C -7F). Similar changes in microstructure were reported when pomegranate peel extracts were incorporated into fish gelatin films, which was attributed to insoluble dietary fibres (Hanani et al. 2019).

Similarly, small heterogeneities in films have been reported when apple peel extract was added to chitosan films (Riaz et al. 2018).

Among the advantages of using AFM in determining the characteristics of nanostructures is that AFM gives magnification in three dimensions: x,y, and z (Ekrami et al. 2021). Users can directly measure the height of a sample feature from an AFM image, while typically, the SEM sample must be cross-sectioned to obtain the height of a feature. AFMs also provide different magnifications in the x, y, and z axes (Nguyen-Tri et al. 2020). According to the AFM results (Fig. 8), the non-formation of AO_{EX} fibres and the creation of beaded structures were also confirmed by the AFM image. Also, the changes in the diameter of PVA nanofibers due to the addition of AO_{EX} can be confirmed in AFM images.

Wettability

Drop shape analysis was used to assess the wettability of the nanofiber's surfaces by evaluating their contact angle. When the contact angle of a surface is less than 90°, it is regarded as hydrophilic; when it is more than this value, it is deemed hydrophobic. In the absence of AO_{EX}, the control (PVA) nanofibers were slightly hydrophilic (θ = 80.8°) (Fig. 9A), which can be attributed to the relatively high polarity of the functional groups. In a similar study, Khan et al. (2019) reported that PVA nanofibers are hydrophilic with a contact angle of 88° (Khan et al. 2019). After adding AO_{EX}, the PVA nanofibers become more hydrophilic (θ = 47.6–73.1°). This decrease in contact angle and increased hydrophilicity can be due to

new interactions and increased hydrophilic groups such as anthocyanins and phenolic compounds. The increased hydrophilicity of the pH-sensitive sensor facilitates the release of H + or OH- from the nanofibers, resulting in a fast colour response as a function of environmental pH (Yuan and Lee 2013). However, the significant changes in the contact angle can be attributed to the effect of adding the extract on the surface roughness, pore size and heterogeneity of the sensors (Hanani et al. 2018), confirmed by the results obtained from the SEM and AFM. In a similar research, Pakolpakçıl et al. (2021) reported a pH-sensitive colourimetric sensor based on alginate/PVA containing anthocyanin extracted from purple cabbage, which is hydrophilic with a contact angle of 45.6 degrees (Pakolpakçıl et al. 2021).

Differential Scanning Calorimetry (DSC)

DSC thermograms of the indicators are shown in Fig. 9B. PVA nanofibers have an endothermic peak in the range of 204-237.5°C as an indication of T_m. In a similar study, Naebe et al. (2007) reported the 200–220°C range as the melting point range of PVA fibres (Naebe et al. 2007). Compared to PVA nanofibers, the T_m values of the PVA-AO_{EX} nanofiber mats have decreased (217.6°C). Since AO_{EX} is hydrophilic, anthocyanin molecules, polyphenols, and flavonoids can act as lubricants and pseudo-plasticisers to move polymer chains and reduce T_m (Yang and Paulson 2000). For polymer compounds to take on a crystalline structure, they must be given enough time to develop their crystals in manufacturing (Kodal et al. 2019). Based on this, the production of nonwoven structures by electrospinning should not lead to a high percentage of crystallisation due to the rapid evaporation of the solvent and consolidation of the chains (Ma et al. 2005). Generally, if the biopolymer and the additive are immiscible, the mixture will have two T_ms, similar to the T_m of both substances in pure form. The appearance of a T_m for the PVA-AO_{EX} nanofiber mats confirms the homogenous dispersion of the AO_{EX} used in the PVA nanofibers structure. Of course, it should be noted that the temperature at which the phase transition occurs depends on the chemical nature of the polymer, the presence or absence of additives, molecular weight, the degree of branching, and the presence of cross-links (Li and Wu 2012).

FTIR analysis

FTIR provides researchers with helpful and valuable information about the structure of polymers and the type of connections between them in different conditions. The FTIR curve of pure compounds and mixtures of compounds may differ, and these differences help the researcher interpret the results. The interaction between functional groups at the molecular level can produce a new bond or a change in the intensity or position (shift) of the created bond (Solghi et al. 2020). The peaks of the FTIR spectra in Fig. 9C confirm the chemical structure of PVA nanofibers, $AO_{EX,}$ and PVA-AO_{EX} 10%v/v nanofiber mats. In the range of 3200–3650 cm^{-1}, a wide bond can be seen due to the absorption by free and bonded OH groups in PVA, which after encapsulation of AO_{EX}, without creating cross-links in PVA and by occupying free hydroxyl groups from the intense, its absorption is increased (Lamarra et al. 2020). In the range of 2730–2860 cm^{-1}, in the spectrum of PVA, stretching vibration caused by H-C and in the spectrum of PVA containing AO_{EX}, stretching vibration caused by O = C-H and C-H group is seen. In the range of 1750

– 1700 cm^{-1} of the spectrum of PVA containing AO_{EX}, the stretching caused by the absorption of unreacted aldehyde end O = C groups on the polymer and the acetate O-C groups of the polymer can be observed in the spectrum of PVA. In the range of 1000–1140 cm^{-1} in the spectrum of PVA, the stretching vibration related to the absorption of O-C-O groups and in the spectrum of PVA containing AO_{EX}, the stretching vibration of acetyl groups (Wen et al. 2016; Dehghani et al. 2020). Also, the links in the range of 1500 cm^{-1} were directed to higher frequencies after adding AO_{EX} and creating a nanocarrier, which has been confirmed in similar research (Solghi et al. 2020). Also, there is no change in the index peaks of the PVA polymer substrate, including the removal of the peak or the appearance of a new peak. In fact, this phenomenon indicates the fact that no type of reaction has occurred during the electrospinning process that leads to the production of new connections and bonds.

Assessment of fish freshness

Fresh fish is one of the perishable marine products. Fish spoilage combines different mechanisms, including fat oxidation, microbial growth and enzyme activity, and enzymatic browning (Li et al. 2021). Psychrophilic bacteria are the leading group of microorganisms that cause aerobic spoilage in fresh fish at low temperatures due to the production of extracellular lipases and proteases (Aghaei et al. 2020). To evaluate the PVA-AO_{EX} 10%v/v nanofibers mat as real-time multi-functional innovative packaging, the changes in TVC, TVB-N, pH, and yellowness index (YI) in fish fillet samples during 14 days of storage at refrigerator temperature (4°C) were investigated. Spoilage of meat and seafood is characterised by increased pH and the formation of volatile nitrogen-based compounds (such as ammonia and amines) due to the breakdown of proteins, usually caused by enzymes and microorganisms (Aghaei et al. 2018). Therefore, colourimetric sensors can change colour in response to changes in pH or ammonia levels and be used as indicators of product freshness/spoilage in packaging (Meral et al. 2019). According to the results of Fig. 10A, after 14 days of fresh fish fillet storage in the refrigerator, TVB-N increased from 3.43 mg/100 g to 38.78 mg/100 g of fish sample. In the fish sample coated with multi-functional smart packaging, after 14 days, the amount of TVB-N reached 27.83 mg/100 g of fish sample. According to previous studies, the acceptable limit of TVB-N for freshwater fish is 20 mg/100 g of sample (Jiang et al. 2020; Moradi et al. 2019). Therefore, in the control sample, on the sixth day of storage in the refrigerator, the amount of TVB-N exceeded the acceptance limit, while the multi-functional innovative packaging increased the acceptance limit of TVB-N up to 8.5 days.

According to the results of Fig. 10B, after 14 days of fresh fish fillet storage in the refrigerator, the TVC increased from $10^{3.37}$ CFU/g to $10^{10.45}$ CFU/g of the fish sample, while the fish sample coated with multi-functional innovative packaging after 14 days of TVC reached $10^{7.90}$ CFU/g of the fish sample. According to previous studies, the acceptable limit of TVC for freshwater fish is 10^{7} CFU/g of sample (Huang et al. 2019). Therefore, in the control sample, on the sixth day of storage in the refrigerator, the TVC exceeded the acceptance limit, while the multi-functional innovative packaging increased the acceptance limit of the TVC up to 9 days.

Our results show that the acceptable limit of TVB-N and TVC are reached simultaneously because the microbial population increases, and thus, secondary metabolites from fish spoilage increase (Ceylan et al. 2017). Figure 10C shows the pH changes of the fish sample and YI of the multi-functional innovative packaging during the storage period. After 9 days of storage at 4°C, the sensor's colour had changed from dull white to dark yellow, which the naked eye detected (Fig. 10D). Also, during this period, the pH of the fish sample entered the alkaline range.

In the present study, the antimicrobial/antioxidant effect and pH sensitivity of anthocyanin-rich PVA-AO_{EX} nanofiber mats as real-time multi-functional innovative packaging were observed simultaneously. The structure of anthocyanins contains multiple phenolic hydroxyl groups, which protect plants from oxidisable components. Due to its unique functionality, it removes free radicals and inhibits lipid peroxidation (Garcia and Blesso 2021). Anthocyanins can absorb oxygen-free radicals in vitro and sequester oxygen and hydroxyl radicals, so they can act as antioxidants to eliminate reactive oxygen species (ROS) (Tena et al. 2020). More recent work has shown that anthocyanins have antibacterial properties. The effects on the bacterial cell membrane could be due to the combination of antibacterial agents with membrane proteins forming hydrogen bonds or through hydrophobic interactions (Cerezo et al. 2020). With this structure, ions required to maintain protein stability were isolated, and the anthocyanin extract was free to accept or donate electrons at the interface of the membrane to make it an antibacterial agent. Anthocyanins can destroy pathogenic bacteria's structure and inhibit its growth (Dong et al. 2022).

It is noteworthy that in similar work, multi-functional colourimetric anthocyanin base sensors were prepared, but because they were used as indicators under packaging, only one of their functions (spoilage monitoring) was used in the final products. For example, Liu et al. (2021) reported pH-sensitive and antibacterial films by incorporating anthocyanins extracted from purple potato or roselle into chitosan/polyvinyl alcohol/nano-ZnO matrix could effectively monitor the spoilage degree of shrimp when film changed from purple to light-green (Liu et al. 2021). Kong et al. (2023) monitored pork freshness using multi-functional pH-sensitive active and intelligent packaging based on highly cross-linked zein/tea tree essential oil-loaded mesoporous silica nanoparticles/anthocyanin-containing blueberry extract (Kong et al. 2023).

Conclusion

AO_{EX} has shown to be a valuable addition to PVA nanofiber mats. Microscopy examination (SEM and AFM) revealed that adding AO_{EX} to the nanofiber mats brought about slight variations in appearance, although other properties (physicochemical, thermal, wettability, and structural properties) were more affected. Also, real-time multi-functional innovative packaging had high antioxidant properties and antibacterial effects against common foodborne pathogens. The anthocyanin-rich AO_{EX} encapsulated with PVA electrospun nanofiber mats, revealing that the real-time multi-functional innovative packaging changed colour from white to brown and, at the same time, exceeded the total viable count (TVC) and total volatile basic nitrogen (TVB-N) acceptance limit of rainbow trout fillet.

Declarations

Author Contribution

Negar Roshani-Dehlaghi and Mohammad Ekrami wrote the main manuscript Zahra Emam-Djomeh and Shima Yousefi supervised the work. All authors reviewed the manuscript.

Funding Declaration

Authors declared that they didn't receive any funding for this research.

Competing Interest declaration

Authors declare that they didn't have any conflict of interest.

References

1. Abd-ElGawad AM, El-Amier YA, Bonanomi G, Gendy AE-NGE, Elgorban AM, Alamery SF & Elshamy AI (2022) Chemical composition of Kickxia aegyptiaca essential oil and its potential antioxidant and antimicrobial activities. Plants. 11(5), 594.
2. Abedi-Firoozjah R, Yousefi S, Heydari M, Seyedfatehi F, Jafarzadeh S, Mohammadi R, Rouhi M & Garavand F (2022) Application of red cabbage anthocyanins as pH-sensitive pigments in smart food packaging and sensors. Polymers. 14(8), 1629.
3. Aghaei Z, Emadzadeh B, Ghorani B & Kadkhodaee R (2018) Cellulose acetate nanofibres containing alizarin as a halochromic sensor for the qualitative assessment of rainbow trout fish spoilage. Food and Bioprocess Technology. 11(5), 1087-1095.
4. Aghaei Z, Ghorani B, Emadzadeh B, Kadkhodaee R & Tucker N (2020) Protein-based halochromic electrospun nanosensor for monitoring trout fish freshness. Food Control. 111, 107065.
5. Ahmed A, Zhang M, Li S & Xu L (2023) Batch Preparation and Characterization of Anthocyanin/CS/PEO Nanofiber Membranes for Food Packages. Fibers and Polymers. 24(9), 3075-3084.
6. Alizadeh-Sani M, Mohammadian E, Rhim J-W & Jafari SM (2020) pH-sensitive (halochromic) smart packaging films based on natural food colorants for the monitoring of food quality and safety. Trends in Food Science & Technology. 105, 93-144.
7. Alizadeh-Sani M, Tavassoli M, McClements DJ & Hamishehkar H (2021a) Multifunctional halochromic packaging materials: Saffron petal anthocyanin loaded-chitosan nanofiber/methyl cellulose matrices. Food Hydrocolloids. 111, 106237.
8. Alizadeh-Sani M, Tavassoli M, Mohammadian E, Ehsani A, Khaniki GJ, Priyadarshi R & Rhim J-W (2021b) pH-responsive color indicator films based on methylcellulose/chitosan nanofiber and barberry anthocyanins for real-time monitoring of meat freshness. International journal of biological macromolecules. 166, 741-750.

9. Baharfar R, Azimi R & Mohseni M (2015) Antioxidant and antibacterial activity of flavonoid-, polyphenol-and anthocyanin-rich extracts from Thymus kotschyanus boiss & hohen aerial parts. Journal of food science and technology. 52, 6777-6783.
10. Bohdanovych T, Belokurova V & Matvieieva N (2023) Varibility of Flavonoid Content, Reducing and Antioxidant Activity in Althaea officinalis L. Hairy Roots. Agrobiodiversity for Improving Nutrition, Health and Life Quality. 7(2).
11. Bonaterra GA, Bronischewski K, Hunold P, Schwarzbach H, Heinrich E-U, Fink C, Aziz-Kalbhenn H, Müller J & Kinscherf R (2020) Anti-inflammatory and Anti-oxidative Effects of Phytohustil® and Root Extract of Althaea officinalis L. on Macrophages in vitro. Frontiers in pharmacology. 11, 290.
12. Cerezo AB, Cătunescu GM, González MM-P, Hornedo-Ortega R, Pop CR, Rusu CC, Chirilă F, Rotar AM, Garcia-Parrilla MC & Troncoso AM (2020) Anthocyanins in blueberries grown in hot climate exert strong antioxidant activity and may be effective against urinary tract bacteria. Antioxidants. 9(6), 478.
13. Ceylan Z, Sengor GFU, Sağdıç O & Yilmaz MT (2017) A novel approach to extend microbiological stability of sea bass (Dicentrarchus labrax) fillets coated with electrospun chitosan nanofibers. LWT-Food Science and Technology. 79, 367-375.
14. Chen H, Yu W, Chen G, Meng S, Xiang Z & He N (2017) Antinociceptive and antibacterial properties of anthocyanins and flavonols from fruits of black and non-black mulberries. Molecules. 23(1), 4.
15. Dehghani S, Noshad M, Rastegarzadeh S, Hojjati M & Fazlara A (2020) Electrospun chia seed mucilage/PVA encapsulated with green cardamonmum essential oils: Antioxidant and antibacterial property. International journal of biological macromolecules. 161, 1-9.
16. Deng H, Zhu J, Tong Y, Kong Y, Tan C, Wang M, Wan M & Meng X (2021) Antibacterial characteristics and mechanisms of action of Aronia melanocarpa anthocyanins against Escherichia coli. LWT. 150, 112018.
17. Dong Y, Yang C, Zhong W, Shu Y, Zhang Y & Yang D (2022) Antibacterial effect and mechanism of anthocyanin from Lycium ruthenicum Murr. Frontiers in microbiology. 13, 974602.
18. Duan M, Yu S, Sun J, Jiang H, Zhao J, Tong C, Hu Y, Pang J & Wu C (2021) Development and characterization of electrospun nanofibers based on pullulan/chitin nanofibers containing curcumin and anthocyanins for active-intelligent food packaging. International journal of biological macromolecules. 187, 332-340.
19. Ebadi Ghareh Koureh L, Ganjloo A, Hamishehkar H & Bimakr M (2023) Fabrication and characterization of costmary essential oil loaded salep-polyvinyl alcohol fast-dissolving electrospun nanofibrous mats. Journal of Food Measurement and Characterization, 1-18.
20. Ekrami A, Ghadermazi M, Ekrami M, Hosseini MA, Emam-Djomeh Z & Hamidi-Moghadam R (2022a) Development and evaluation of Zhumeria majdae essential oil-loaded nanoliposome against multidrug-resistant clinical pathogens causing nosocomial infection. Journal of Drug Delivery Science and Technology. 69, 103148.

21. Ekrami M, Ekrami A, Esmaeily R & Emam-Djomeh Z (2022b) Nanotechnology-based Formulation for Alternative Medicines and Natural Products: An Introduction with Clinical Studies. Biopolymers in Nutraceuticals and Functional Foods, 545-580.
22. Ekrami M, Ekrami A, Hosseini MA & Emam-Djomeh Z (2022c) Characterization and optimization of salep mucilage bionanocomposite films containing Allium jesdianum Boiss. Nanoliposomes for antibacterial food packaging utilization. Molecules. 27(20), 7032.
23. Ekrami M, Ekrami A, Moghadam RH, Joolaei-Ahranjani P & Emam-Djomeh Z (2022d) Food-based Polymers for Encapsulation and Delivery of Bioactive Compounds. In: Biopolymers in Nutraceuticals and Functional Foods. p^pp 488-544. The Royal Society of Chemistry.
24. Ekrami M, Emam-Djomeh Z, Ghoreishy SA, Najari Z & Shakoury N (2019) Characterization of a high-performance edible film based on Salep mucilage functionalized with pennyroyal (Mentha pulegium). International journal of biological macromolecules. 133, 529-537.
25. Ekrami M, Emam-Djomeh Z, Joolaei-Ahranjani P, Mahmoodi S & Khaleghi S (2021) Eco-friendly UV protective bionanocomposite based on Salep-mucilage/flower-like ZnO nanostructures to control photo-oxidation of kilka fish oil. International journal of biological macromolecules. 168, 591-600.
26. Ekrami M, Roshani-Dehlaghi N, Ekrami A, Shakouri M & Emam-Djomeh Z (2022e) pH-Responsive Color Indicator of Saffron (Crocus sativus L.) Anthocyanin-Activated Salep Mucilage Edible Film for Real-Time Monitoring of Fish Fillet Freshness. Chemistry. 4(4), 1360-1381.
27. Elmastas M, Ozturk L, Gokce I, Erenler R & Aboul-Enein HY (2004) Determination of antioxidant activity of marshmallow flower (Althaea officinalis L.). Analytical letters. 37(9), 1859-1869.
28. Emam-Djomeh Z, Ekrami M, Ekrami & Ali (2023) Overview of Types of Materials Used for Food Component Encapsulation. Materials Science and Engineering in Food Product Development, 73-92.
29. Emam-Djomeh Z, Moghaddam A & Yasini Ardakani SA (2015) Antimicrobial activity of pomegranate (Punica granatum L.) peel extract, physical, mechanical, barrier and antimicrobial properties of pomegranate peel extract-incorporated sodium caseinate film and application in packaging for ground beef. Packaging Technology and Science. 28(10), 869-881.
30. Garcia C & Blesso CN (2021) Antioxidant properties of anthocyanins and their mechanism of action in atherosclerosis. Free Radical Biology and Medicine. 172, 152-166.
31. Goodarzi MM, Moradi M, Tajik H, Forough M, Ezati P & Kuswandi B (2020) Development of an easy-to-use colorimetric pH label with starch and carrot anthocyanins for milk shelf life assessment. International journal of biological macromolecules. 153, 240-247.
32. Habibi M, Golmakani MT, Mesbahi G, Majzoobi M & Farahnaky A (2015) Ultrasound-accelerated debittering of olive fruits. Innovative Food Science & Emerging Technologies. 31, 105-115.
33. Hanani ZN, Husna AA, Syahida SN, Khaizura MN & Jamilah B (2018) Effect of different fruit peels on the functional properties of gelatin/polyethylene bilayer films for active packaging. Food Packaging and Shelf Life. 18, 201-211.
34. Hanani ZN, Yee FC & Nor-Khaizura M (2019) Effect of pomegranate (Punica granatum L.) peel powder on the antioxidant and antimicrobial properties of fish gelatin films as active packaging.

Food Hydrocolloids. 89, 253-259.
35. He Y, Lu L, Lin Y, Li R, Yuan Y, Lu X, Zou Y, Zhou W, Wang Z & Li J (2022) Intelligent pH-sensing film based on polyvinyl alcohol/cellulose nanocrystal with purple cabbage anthocyanins for visually monitoring shrimp freshness. International journal of biological macromolecules. 218, 900-908.
36. Hoffmann TG, Angioletti BL, Bertoli SL & de Souza CK (2022) Intelligent pH-sensing film based on jaboticaba peels extract incorporated on a biopolymeric matrix. Journal of food science and technology. 59(3), 1001-1010.
37. Huang S, Xiong Y, Zou Y, Dong Q, Ding F, Liu X & Li H (2019) A novel colorimetric indicator based on agar incorporated with Arnebia euchroma root extracts for monitoring fish freshness. Food Hydrocolloids. 90, 198-205.
38. Jeyaraj EJ, Lim YY & Choo WS (2022) Antioxidant, cytotoxic, and antibacterial activities of Clitoria ternatea flower extracts and anthocyanin-rich fraction. Scientific Reports. 12(1), 14890.
39. Jiang G, Hou X, Zeng X, Zhang C, Wu H, Shen G, Li S, Luo Q, Li M & Liu X (2020) Preparation and characterization of indicator films from carboxymethyl-cellulose/starch and purple sweet potato (Ipomoea batatas (L.) lam) anthocyanins for monitoring fish freshness. International journal of biological macromolecules. 143, 359-372.
40. Karimi S, Ghanbarzadeh B, Roufegarinejad L & Falcone PM (2021) Polysaccharide extracted from Althaea officinalis L. root: New studies of structural, rheological and antioxidant properties. Carbohydrate Research. 510, 108438.
41. Khan MQ, Kharaghani D, Nishat N, Shahzad A, Hussain T, Khatri Z, Zhu C & Kim IS (2019) Preparation and characterizations of multifunctional PVA/ZnO nanofibers composite membranes for surgical gown application. Journal of materials research and technology. 8(1), 1328-1334.
42. Kodal M, Karakaya N, Wis AA & Ozkoc G (2019) Thermal properties (DSC, TMA, TGA, DTA) of rubber nanocomposites containing carbon nanofillers. In: Carbon-Based Nanofillers and Their Rubber Nanocomposites. p^pp 325-366. Elsevier.
43. Kong J, Ge X, Sun Y, Mao M, Yu H, Chu R & Wang Y (2023) Multi-functional pH-sensitive active and intelligent packaging based on highly cross-linked zein for the monitoring of pork freshness. Food chemistry. 404, 134754.
44. Krüger E, Will F, Kumar K, Celejewska K, Chartier P, Masny A, Mott D, Petit A, Savini G & Sønsteby A (2021) Influence of post-flowering climate conditions on anthocyanin profile of strawberry cultivars grown from north to south Europe. Applied Sciences. 11(3), 1326.
45. Lamarra J, Calienni MN, Rivero S & Pinotti A (2020) Electrospun nanofibers of poly (vinyl alcohol) and chitosan-based emulsions functionalized with cabreuva essential oil. International journal of biological macromolecules. 160, 307-318.
46. Li M & Wu Z (2012) A review of intercalation composite phase change material: preparation, structure and properties. Renewable and Sustainable Energy Reviews. 16(4), 2094-2101.
47. Li T, Li J, Hu W & Li X (2013) Quality enhancement in refrigerated red drum (Sciaenops ocellatus) fillets using chitosan coatings containing natural preservatives. Food chemistry. 138(2-3), 821-826.

48. Li T, Wang D, Ren L, Mei J, Xu Y & Li J (2021) Preparation of pH-sensitive polylactic acid-naringin coaxial electrospun fiber membranes for maintaining and monitoring salmon freshness. International journal of biological macromolecules. 188, 708-718.
49. Liu J, Huang J, Ying Y, Hu L & Hu Y (2021) pH-sensitive and antibacterial films developed by incorporating anthocyanins extracted from purple potato or roselle into chitosan/polyvinyl alcohol/nano-ZnO matrix: Comparative study. International journal of biological macromolecules. 178, 104-112.
50. Liu J, Tan Y, Zhou H, Mundo JLM & McClements DJ (2019) Protection of anthocyanin-rich extract from pH-induced color changes using water-in-oil-in-water emulsions. Journal of Food Engineering. 254, 1-9.
51. Lv H, Wang C, He D, Zhao H, Zhao M, Xu E, Jin Z, Yuan C, Guo L & Wu Z (2024) Intelligent food tag: A starch-anthocyanin-based pH-sensitive electrospun nanofiber mat for real-time food freshness monitoring. International journal of biological macromolecules. 256, 128384.
52. Ma Z, Kotaki M & Ramakrishna S (2005) Electrospun cellulose nanofiber as affinity membrane. Journal of membrane science. 265(1-2), 115-123.
53. Mahboubi M (2020) Marsh mallow (Althaea officinalis L.) and its potency in the treatment of cough. Complementary medicine research. 27(3), 174-183.
54. Meral R, Alav A, Karakas C, Dertli E, Yilmaz MT & Ceylan Z (2019) Effect of electrospun nisin and curcumin loaded nanomats on the microbial quality, hardness and sensory characteristics of rainbow trout fillet. LWT. 113, 108292.
55. Miguel MG (2011) Anthocyanins: Antioxidant and/or anti-inflammatory activities. Journal of applied pharmaceutical science(Issue), 07-15.
56. Mirzakhani M, Ekrami M & Moini S (2018) Chemical composition, total phenolic content and antimicrobial activities of Zhumeria majdae. Journal of Food and Bioprocess Engineering (JFBE). 1, 8.
57. Moradi M, Tajik H, Almasi H, Forough M & Ezati P (2019) A novel pH-sensing indicator based on bacterial cellulose nanofibers and black carrot anthocyanins for monitoring fish freshness. Carbohydrate polymers. 222, 115030.
58. Mousavi SF, Razavi SM & Koocheki A (2019) Marshmallow (Althaea officinalis) Flower Gum. Emerging Natural Hydrocolloids: Rheology and Functions, 397-423.
59. Naebe M, Lin T, Tian W, Dai L & Wang X (2007) Effects of MWNT nanofillers on structures and properties of PVA electrospun nanofibres. Nanotechnology. 18(22), 225605.
60. Nguyen-Tri P, Ghassemi P, Carriere P, Nanda S, Assadi AA & Nguyen DD (2020) Recent applications of advanced atomic force microscopy in polymer science: A review. Polymers. 12(5), 1142.
61. Omidi A, Rahdari S & Fard MH (2014) A preliminary study on antioxidant activities of saffron petal extracts in lambs. Veterinary Science Development. 4(1).
62. Pakolpakçıl A, Osman B, Göktalay G, Özer ET, Şahan Y, Becerir B & Karaca E (2021) Design and in vivo evaluation of alginate-based pH-sensing electrospun wound dressing containing anthocyanins.

Journal of Polymer Research. 28, 1-13.

63. PAŞCA C, MĂRGHITAŞ LA, BOBIŞ O, DEZMIREAN DS, Mărgăoan R & MUREŞAN C (2016) Total Content of Polyphenols and Antioxidant Activity of Different Melliferous Plants. Bulletin of the University of Agricultural Sciences & Veterinary Medicine Cluj-Napoca Animal Science & Biotechnologies. 73(1).
64. Riaz A, Lei S, Akhtar HMS, Wan P, Chen D, Jabbar S, Abid M, Hashim MM & Zeng X (2018) Preparation and characterization of chitosan-based antimicrobial active food packaging film incorporated with apple peel polyphenols. International Journal of Biological Macromolecules. 114, 547-555.
65. Saati EA, Pusparini AD, Wachid M & Winarsih S (2018) The anthocyanin pigment extract from red rose as antibacterial agent. Malaysian Journal of Fundamental and Applied Sciences, 184-187.
66. Sadighara P, Gharibi S, Jafari AM, Khaniki GJ & Salari S (2012) The antioxidant and Flavonoids contents of Althaea officinalis L. flowers based on their color. Avicenna journal of phytomedicine. 2(3), 113.
67. Shakouri M, Salami M, Lim L-T, Ekrami M, Mohammadian M, Askari G, Emam-Djomeh Z & McClements DJ (2023) Development of active and intelligent colorimetric biopolymer indicator: Anthocyanin-loaded gelatin-basil seed gum films. Journal of Food Measurement and Characterization. 17(1), 472-484.
68. Solghi S, Emam-Djomeh Z, Fathi M & Farahani F (2020) The encapsulation of curcumin by whey protein: Assessment of the stability and bioactivity. Journal of Food Process Engineering. 43(6), e13403.
69. Sun X-h, Zhou T-t, Wei C-h, Lan W-q, Zhao Y, Pan Y-j & Wu VC (2018) Antibacterial effect and mechanism of anthocyanin rich Chinese wild blueberry extract on various foodborne pathogens. Food Control. 94, 155-161.
70. Sutharut J & Sudarat J (2012) Total anthocyanin content and antioxidant activity of germinated colored rice. International Food Research Journal. 19(1).
71. Tabarsa M, Anvari M, Joyner HS, Behnam S & Tabarsa A (2017) Rheological behavior and antioxidant activity of a highly acidic gum from Althaea officinalis flower. Food Hydrocolloids. 69, 432-439.
72. Tassanawat S, Phandee A, Magaraphan R, Nithitanakul M & Manuspiya H pH-sensitive PP/clay nanocomposites for beverage smart packaging. In: 2007 2nd IEEE International Conference on Nano/Micro Engineered and Molecular Systems, 2007. IEEE, pp 478-482.
73. Tena N, Martín J & Asuero AG (2020) State of the art of anthocyanins: Antioxidant activity, sources, bioavailability, and therapeutic effect in human health. Antioxidants. 9(5), 451.
74. Wen P, Zhu D-H, Wu H, Zong M-H, Jing Y-R & Han S-Y (2016) Encapsulation of cinnamon essential oil in electrospun nanofibrous film for active food packaging. Food Control. 59, 366-376.
75. Xue T, Ruan K, Tang Z, Duan J & Xu H (2023) Isolation, structural properties, and bioactivities of polysaccharides from Althaea officinalis Linn.: A review. International journal of biological

macromolecules, 125098.
76. Yang L & Paulson A (2000) Mechanical and water vapour barrier properties of edible gellan films. Food Research International. 33(7), 563-570.
77. Yuan Y & Lee TR (2013) Contact angle and wetting properties. In: Surface science techniques. p^pp 3-34. Springer.
78. Zhai X, Shi J, Zou X, Wang S, Jiang C, Zhang J, Huang X, Zhang W & Holmes M (2017) Novel colorimetric films based on starch/polyvinyl alcohol incorporated with roselle anthocyanins for fish freshness monitoring. Food Hydrocolloids. 69, 308-317.
79. Zhang L, Hao M, Yao L, Xing C, Wen Q, Zhang Z, Yu J, Wang J, Xing D & Zheng T (2023) Sericin “hairpin structure”-based multifunctional anthocyanin nanoencapsulation for remodeling ROS-dependent cutaneous wound healing. Chemical Engineering Journal. 475, 145863.
80. Zhang X, Liu Y, Yong H, Qin Y, Liu J & Liu J (2019) Development of multifunctional food packaging films based on chitosan, TiO2 nanoparticles and anthocyanin-rich black plum peel extract. Food Hydrocolloids. 94, 80-92.

Figures

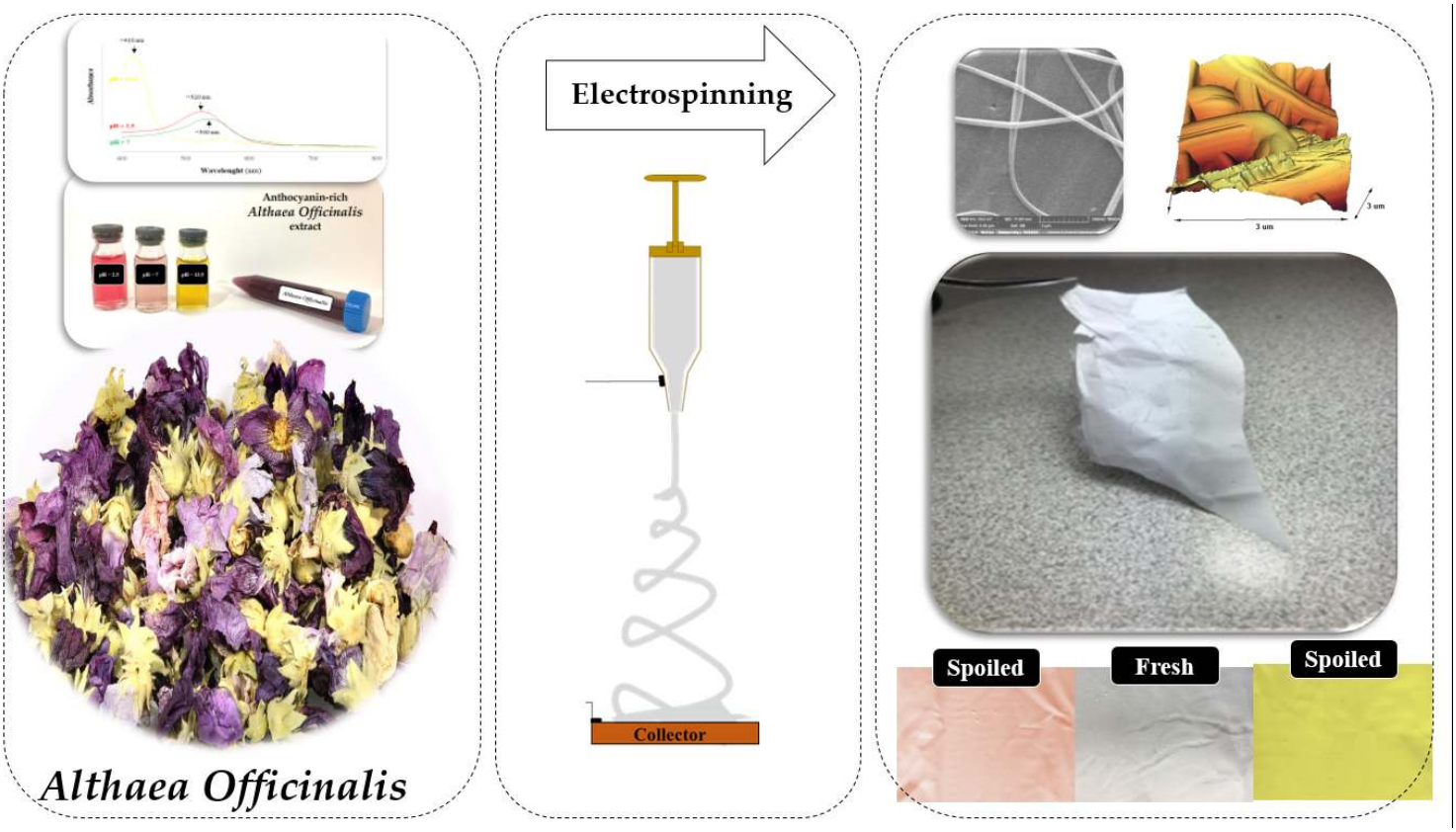

Figure 1

Schematic representation of the electrospinning technique utilised for obtaining AO_{EX}-loaded PVA nanofiber as real-time multi-functional innovative packaging of rainbow trout fillet

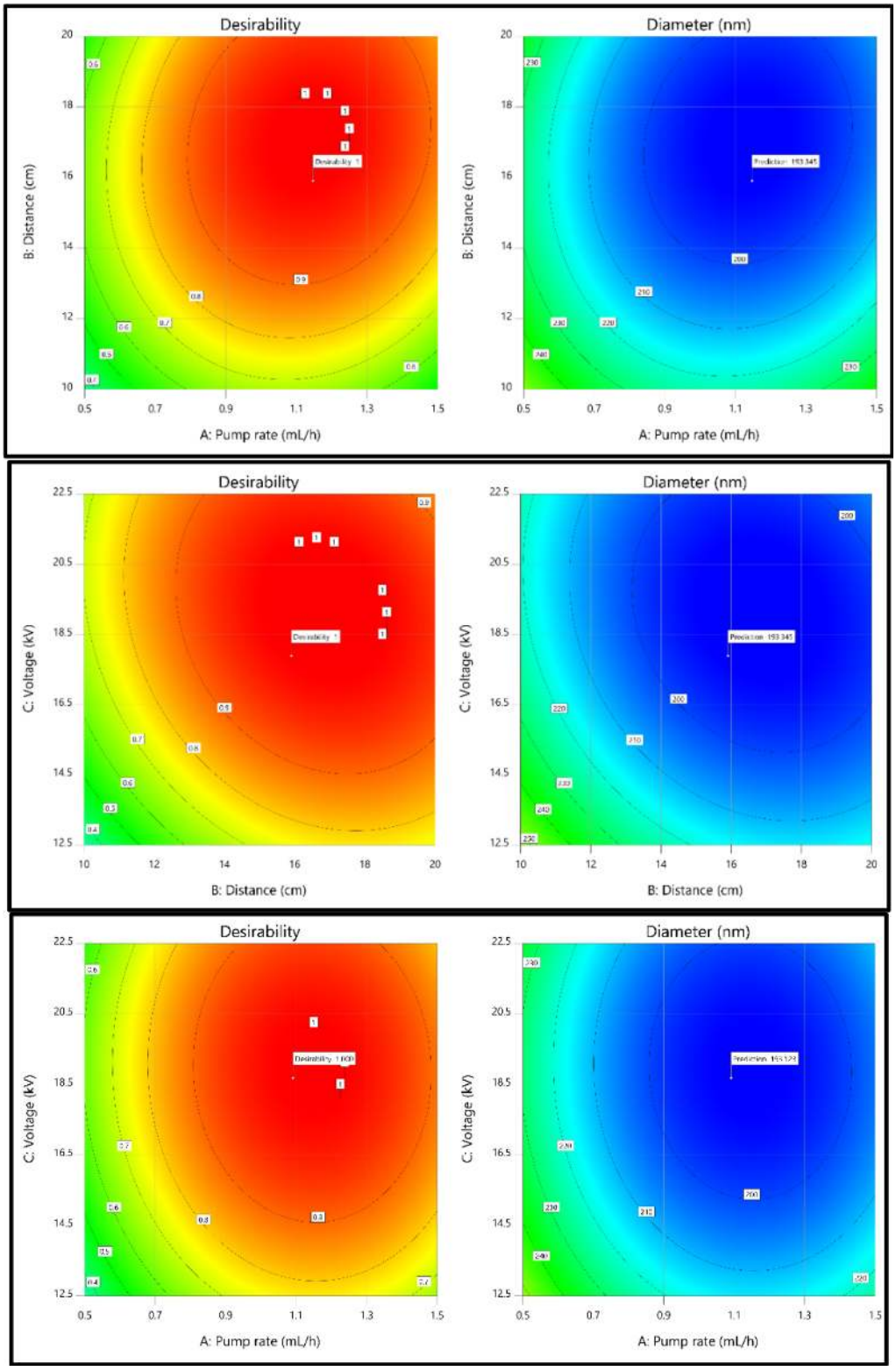

Figure 2

Contour plots for the diameter and desirability of the optimum conditions for fabricating PVA nanofibers

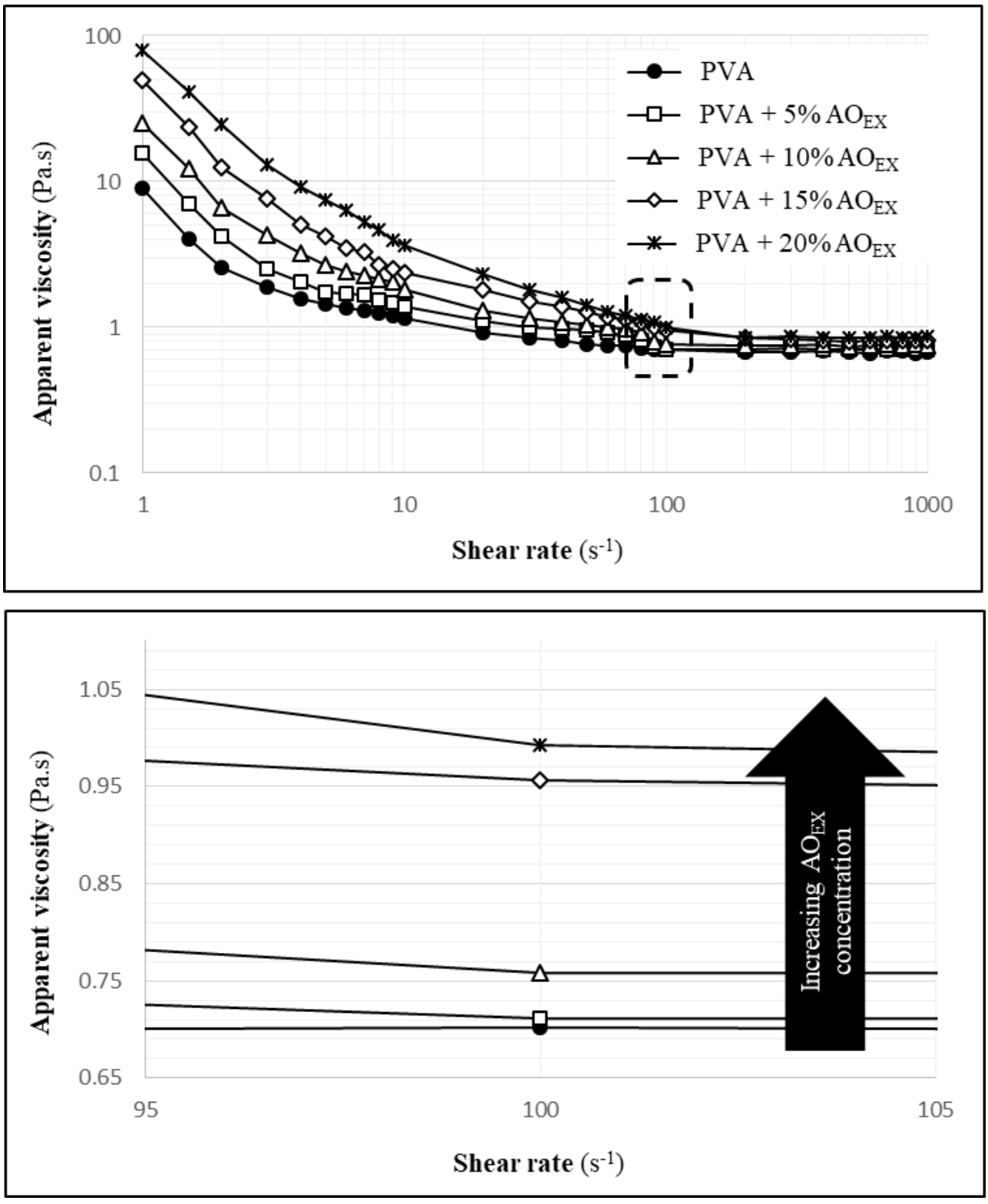

Figure 3

Apparent viscosity–shear rate profile of PVA and PVA-AO_{EX} solutions

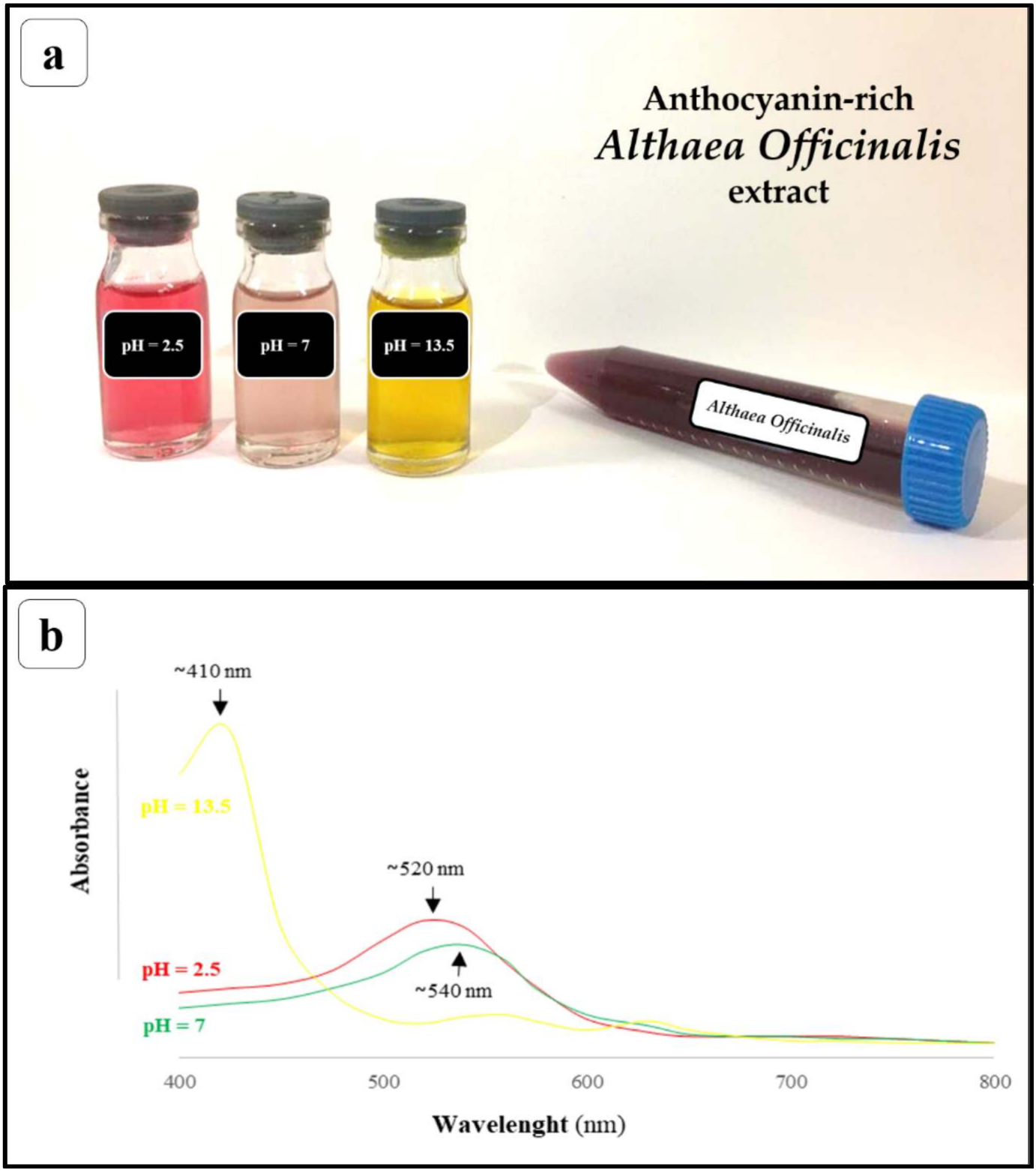

Figure 4

The pH-dependence of (A) solution colour variations and (B) UV-VIS spectra of AO_{EX} were measured in various buffer solutions

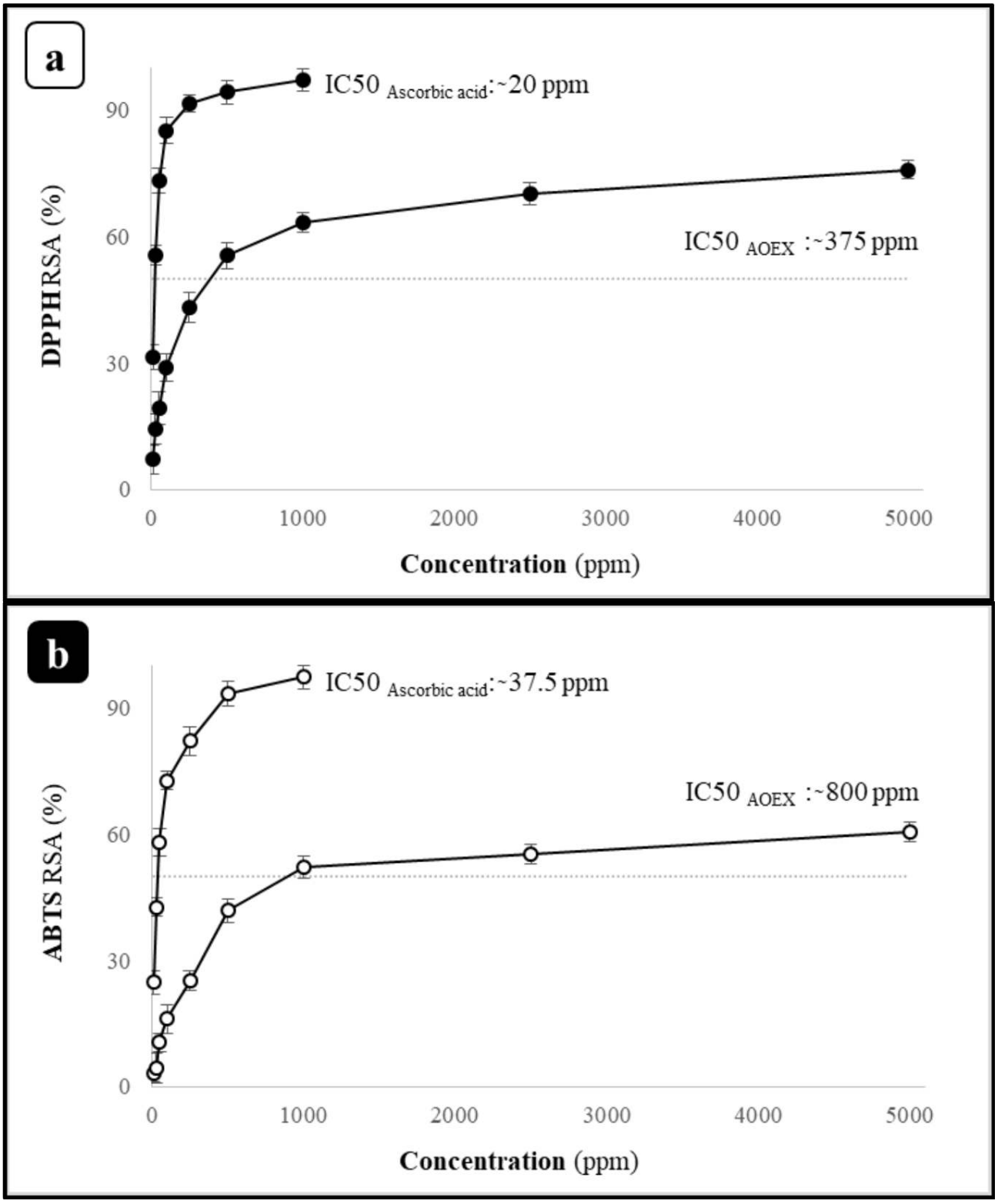

Figure 5

Antioxidant activity of various concentrations and IC_{50} of AO_{EX} and ascorbic acid based on the radical scavenging of (A) DPPH and (B) ABTS

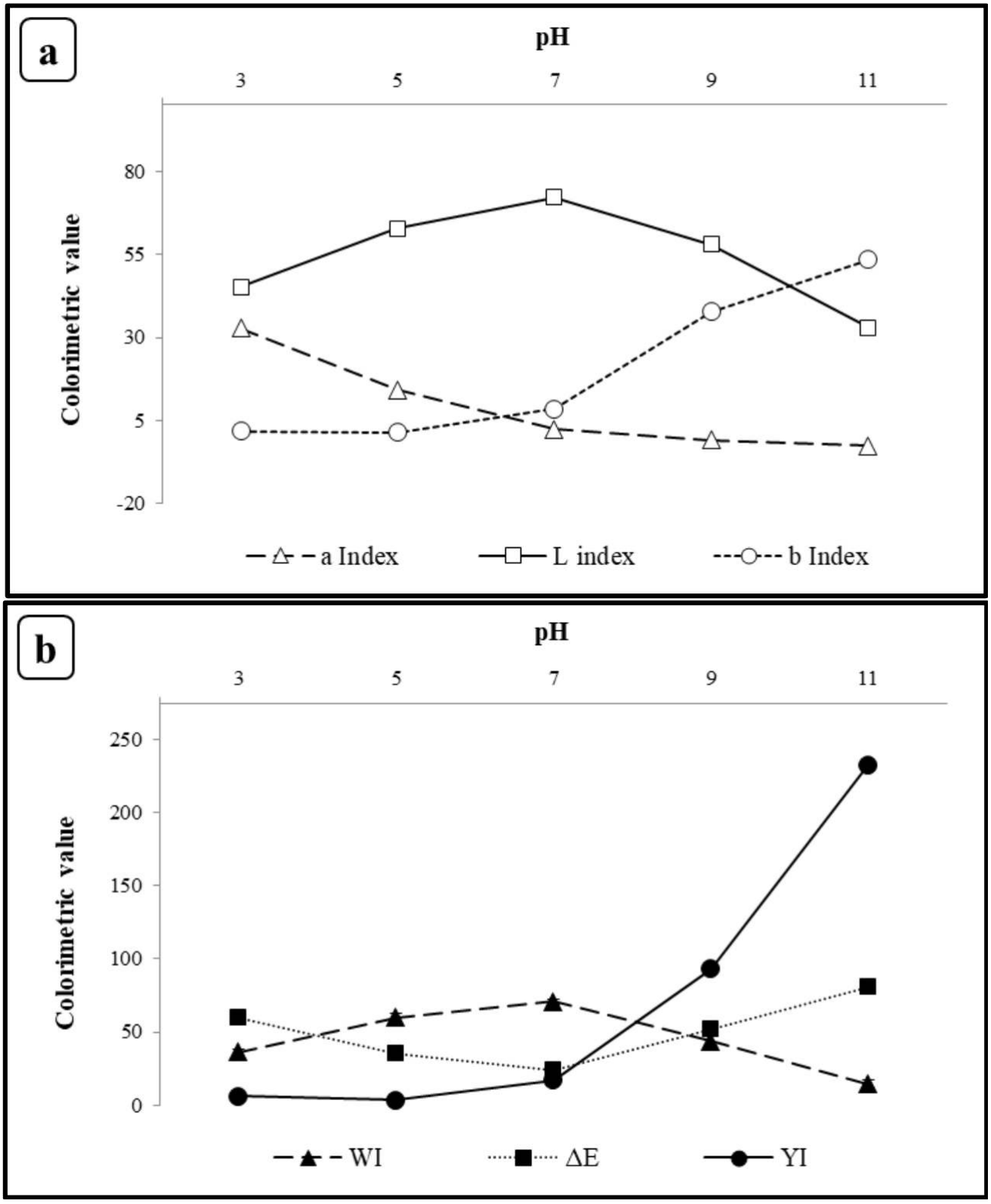

Figure 6

Effect of pH variation on color sensitivity PVA-AO_{EX} 10 %v/v nanofiber mats: (A) L^*, a^*, and b^* index (B) ΔE, WI, and YI

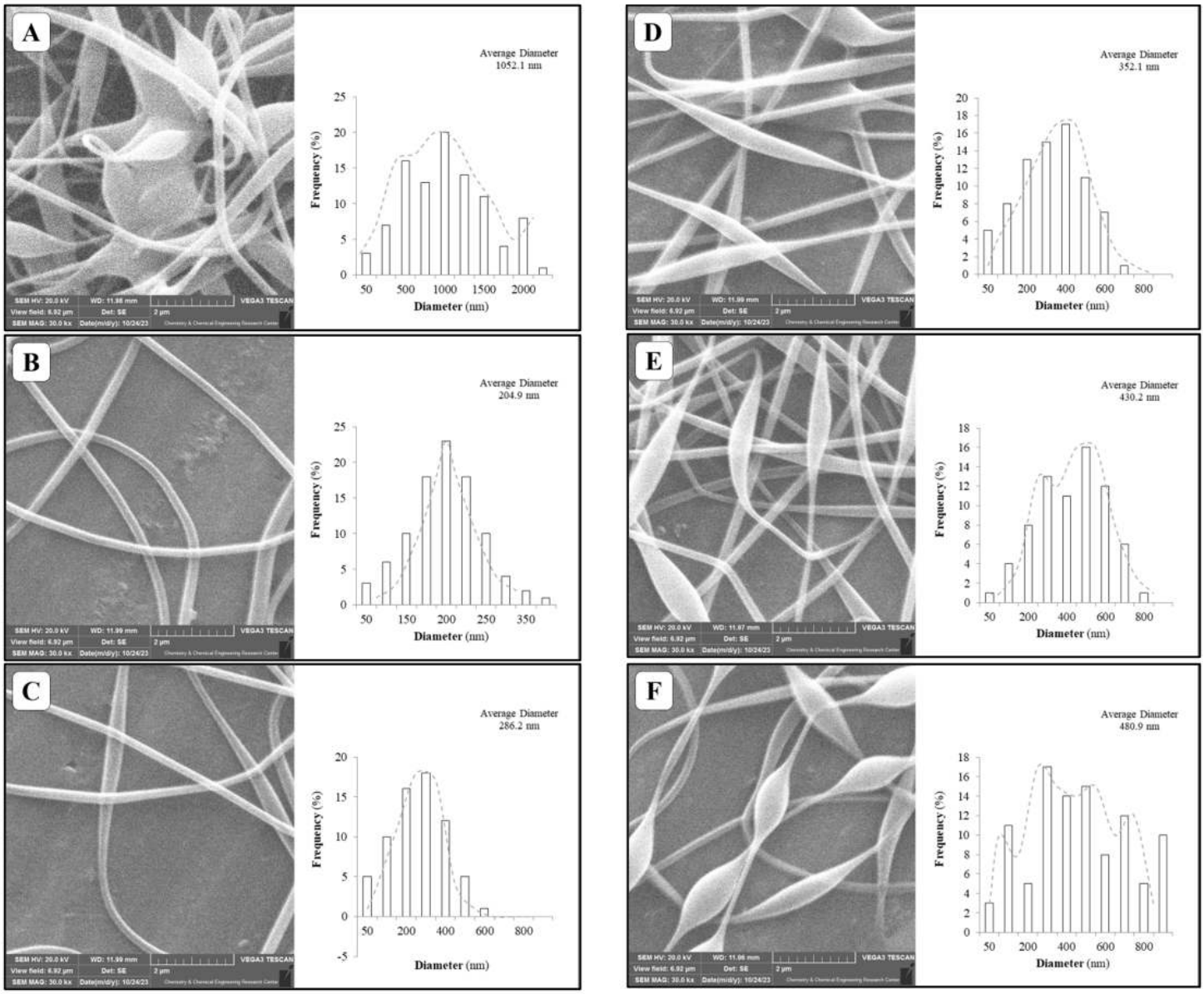

Figure 7

SEM images of the surface and size distribution of (A) AO_{EX}, (B) control - PVA nanofibers and PVA-AO_{EX} nanofiber mats containing (C) 5 %v/v, (D) 10 %v/v, (E) 15 %v/v, (F) 20 %v/v of AO_{EX}

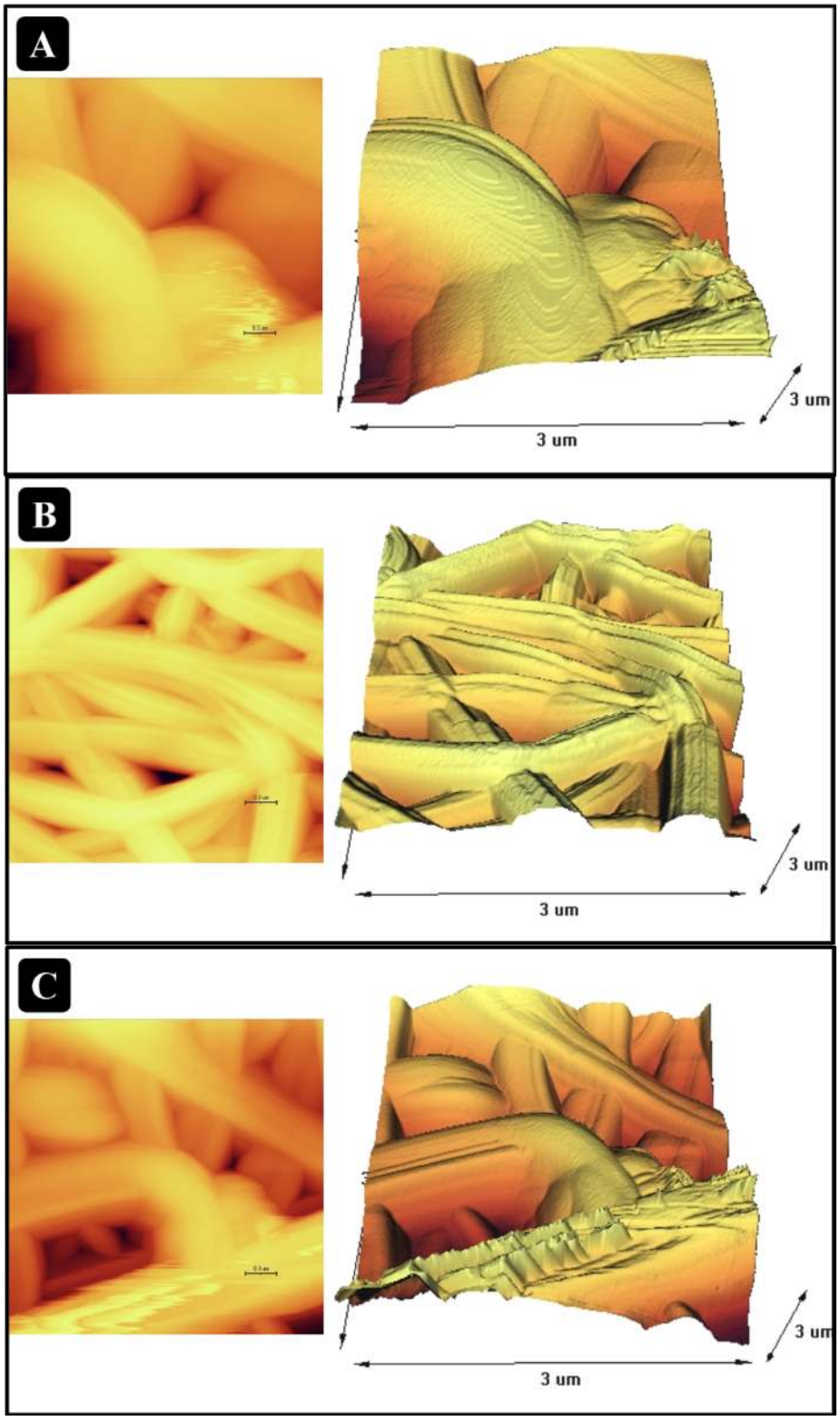

Figure 8

AFM 3D images of (A) $AO_{EX,}$ (B) control - PVA nanofibers and (C) PVA-AO_{EX} 10 %v/v nanofiber mats

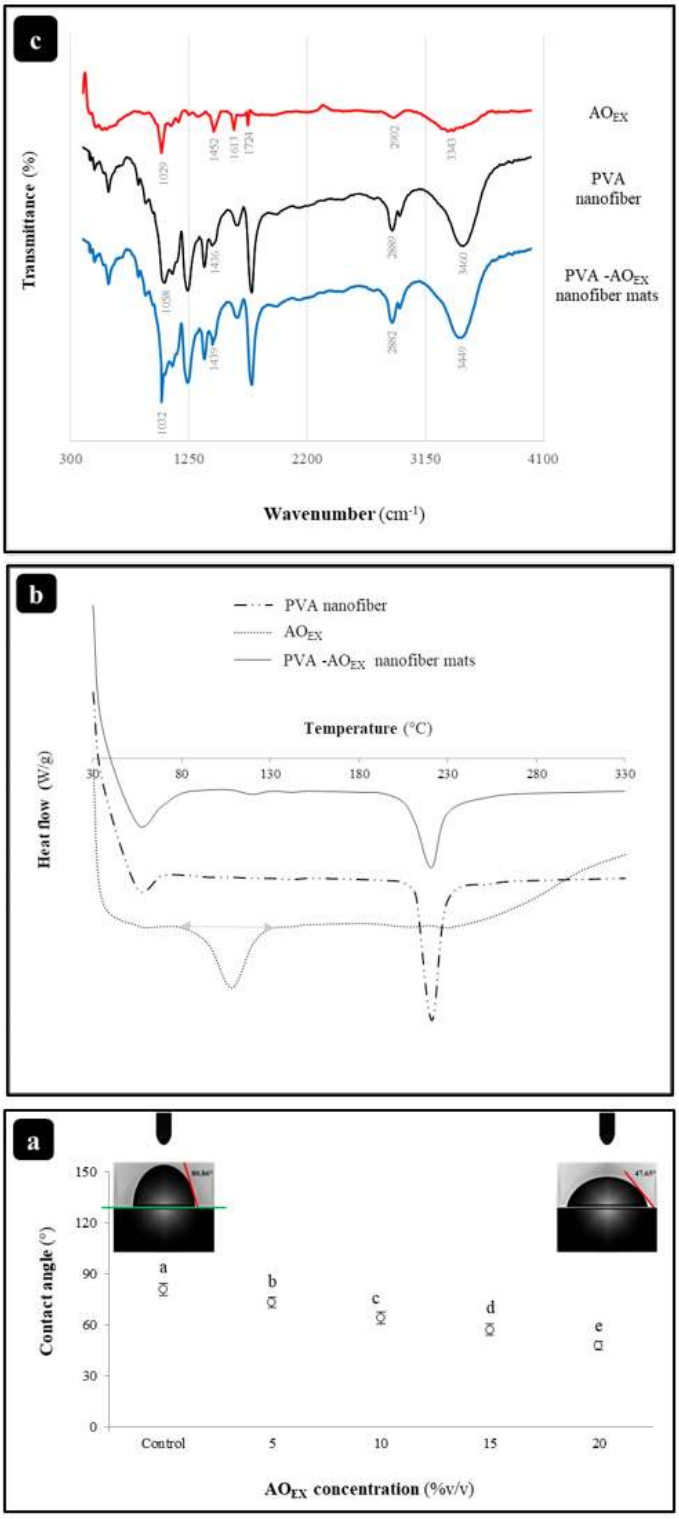

Figure 9

(A) Effect of AO_{EX} variation on the contact angle of PVA-AO_{EX} nanofiber mats (B) DSC thermograms and (C) FTIR spectra of AO_{EX}, PVA nanofibers and PVA-AO_{EX} 10 %v/v nanofiber mats

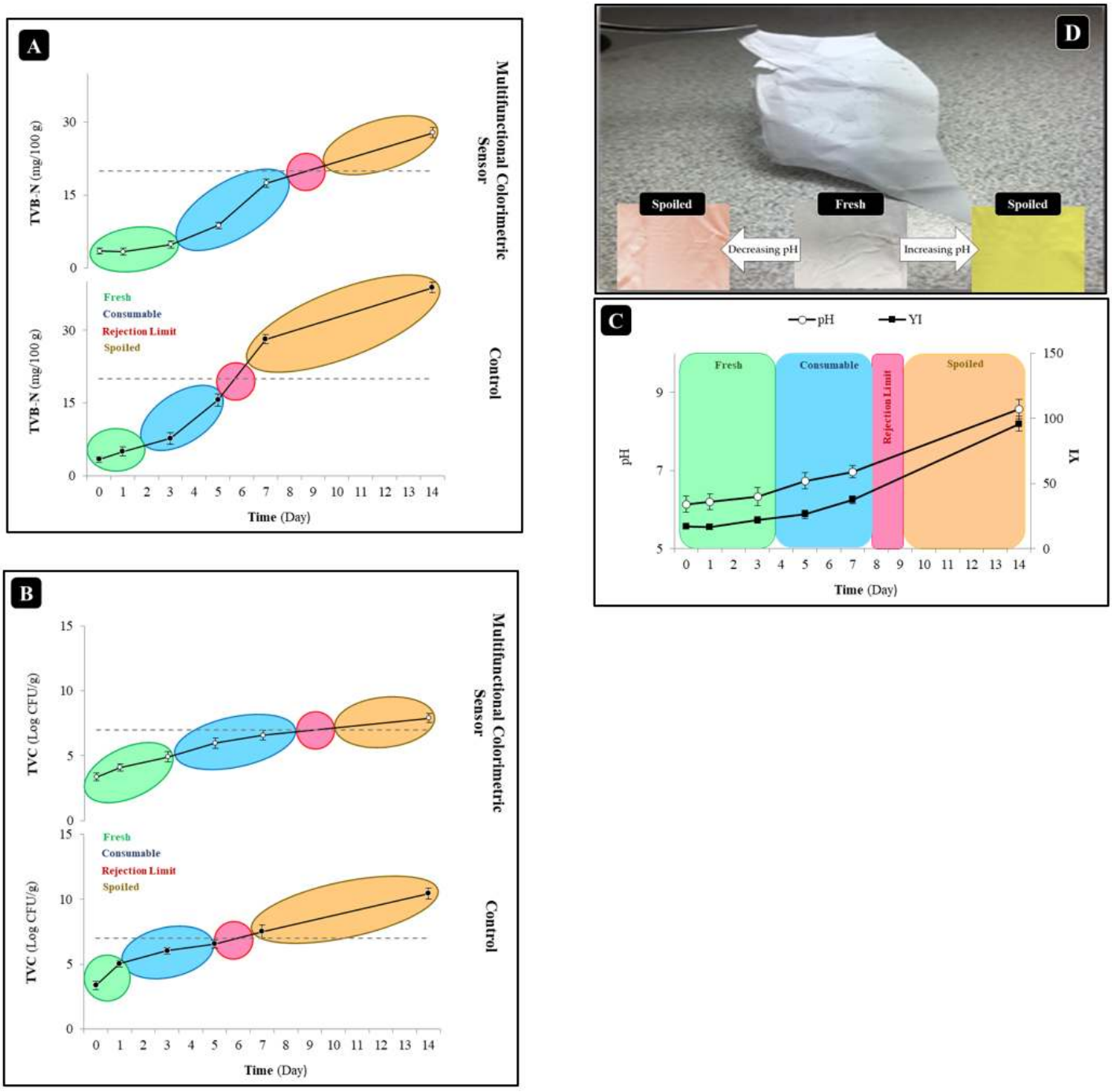

Figure 10

Changes of (A) TVB-N, (B) TVC and (C) pH/ΔE values of rainbow trout fillet during storage at 4 °C using real-time multi-functional innovative packaging

Supplementary Files

This is a list of supplementary files associated with this preprint. Click to download.

- GraphicalAbstract4.docx